Reports on Progress in **Physics**

PURPOSE-LED PUBLISHING™

PAPER • **OPEN ACCESS**

Test of lepton flavor universality in $B^{\pm} \to K^{\pm}\mu^{+}\mu^{-}$ and $B^{\pm} \to K^{\pm}e^{+}e^{-}$ decays in proton-proton collisions at $\sqrt{s} = 13\,\text{TeV}$

To cite this article: The CMS Collaboration 2024 *Rep. Prog. Phys.* **87** 077802

OPEN ACCESS
IOP Publishing
Reports on Progress in Physics
Rep. Prog. Phys. **87** (2024) 077802 (36pp)
https://doi.org/10.1088/1361-6633/ad4e65

Test of lepton flavor universality in $B^{\pm} \to K^{\pm}\mu^{+}\mu^{-}$ and $B^{\pm} \to K^{\pm}e^{+}e^{-}$ decays in proton-proton collisions at $\sqrt{s} = 13\,\text{TeV}$

The CMS Collaboration

CERN, Geneva, Switzerland

E-mail: cms-publication-committee-chair@cern.ch

Received 12 January 2024, revised 8 May 2024
Accepted for publication 21 May 2024
Published 3 July 2024

Corresponding editor: Dr Paul Mabey

Abstract

A test of lepton flavor universality in $B^{\pm} \to K^{\pm}\mu^{+}\mu^{-}$ and $B^{\pm} \to K^{\pm}e^{+}e^{-}$ decays, as well as a measurement of differential and integrated branching fractions of a nonresonant $B^{\pm} \to K^{\pm}\mu^{+}\mu^{-}$ decay are presented. The analysis is made possible by a dedicated data set of proton-proton collisions at $\sqrt{s} = 13\,\text{TeV}$ recorded in 2018, by the CMS experiment at the LHC, using a special high-rate data stream designed for collecting about 10 billion unbiased b hadron decays. The ratio of the branching fractions $\mathcal{B}(B^{\pm} \to K^{\pm}\mu^{+}\mu^{-})$ to $\mathcal{B}(B^{\pm} \to K^{\pm}e^{+}e^{-})$ is determined from the measured double ratio $R(K)$ of these decays to the respective branching fractions of the $B^{\pm} \to J/\psi K^{\pm}$ with $J/\psi \to \mu^{+}\mu^{-}$ and $e^{+}e^{-}$ decays, which allow for significant cancellation of systematic uncertainties. The ratio $R(K)$ is measured in the range $1.1 < q^2 < 6.0\,\text{GeV}^2$, where q is the invariant mass of the lepton pair, and is found to be $R(K) = 0.78^{+0.47}_{-0.23}$, in agreement with the standard model expectation $R(K) \approx 1$. This measurement is limited by the statistical precision of the electron channel. The integrated branching fraction in the same q^2 range, $\mathcal{B}(B^{\pm} \to K^{\pm}\mu^{+}\mu^{-}) = (12.42 \pm 0.68) \times 10^{-8}$, is consistent with the present world-average value and has a comparable precision.

Keywords: CMS, B physics, lepton flavor universality, B meson, b to sll transitions

1. Introduction

In the standard model (SM) of particle physics [1–3], the charged leptons (electrons P, muons μ, and τ leptons) have identical couplings to the gauge bosons and thus exhibit a similar behavior, up to the kinematic differences related to their different masses. This is commonly known as lepton flavor universality (LFU). Several tests of LFU have been performed in W and Z boson decays, which are generally found to be in excellent agreement with the SM predictions [4]. The only hint of possible LFU violation (LFUV), at 2.7 standard deviations (σ) in the decay of W bosons to τ vs. light leptons from the CERN LEP era [5], was ruled out by the ATLAS [6] and CMS [7] experiments at the CERN LHC.

Rare b hadron decays provide an excellent and complementary environment to test LFU. In particular, the $B^{+} \to K^{+}\ell^{+}\ell^{-}$ process where a bottom antiquark ($\bar{b}$) decays into a strange antiquark ($\bar{s}$) and a lepton ($\ell = \mu$ or P) pair is forbidden at tree level and only proceeds via loop diagrams, e.g., the one shown in figure 1(left). Therefore, the SM branching fractions

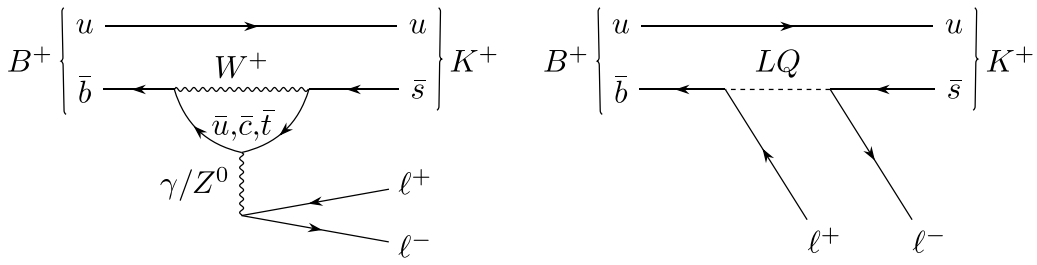

Figure 1. Representative Feynman diagrams for the decay of a B^+ meson into a K^+ meson and a lepton pair in the SM (left) and in a BSM scenario that introduces a leptoquark (LQ) with flavor-dependent couplings (right).

($\mathcal{B}$) for these decays are very small ($\sim 10^{-7}$) [4]. This process is referred to as a $\bar{b} \to \bar{s}\ell^+\ell^-$ transition (in what follows, the charge-conjugated states are implied unless explicitly stated otherwise).

Since both the electron and muon masses are negligible with respect to the B meson mass, the available phase space for the two decays ($B^+ \to K^+\mu^+\mu^-$ and $B^+ \to K^+e^+e^-$) is the same to an excellent approximation, which makes the ratio of these branching fractions very close to unity in the SM. On the other hand, beyond-the-SM (BSM) physics processes could modify the corresponding branching fractions differently for different lepton species, as illustrated in figure 1(right) for the case of a leptoquark with flavor-dependent couplings, thus resulting in LFUV in $\bar{b} \to \bar{s}\ell^+\ell^-$ transitions. A recent review of various BSM models describing LFUV in B meson decays can be found in [8] and references therein, as well as in an extensive list of references in [9].

A number of tests of LFUV have been performed at the B and charm factories [10–18], as well as at the LHC. Over the past decade, the LHCb experiment has reported mounting evidence for LFUV in $B^+ \to K^+\ell^+\ell^-$ [9, 19, 20], $B^0 \to K^*(892)^0\ell^+\ell^-$ [21], $B^0 \to K^0_S\ell^+\ell^-$, and $B^+ \to K^*(892)^+\ell^+\ell^-$ [22] decays with the significance reaching 3.1σ in the first channel [9]. In these analyses the muon decays are measured to be suppressed compared to the electron ones. In addition, multiple measurements of branching fractions of several $\bar{b} \to \bar{s}\mu^+\mu^-$ decays by LHCb indicate their suppression with respect to the available SM predictions [23–26]. These state-of-the-art predictions reflect a significant recent theoretical progress in understanding of the $\bar{b} \to \bar{s}\ell^+\ell^-$ transitions. Nevertheless, full control of nonperturbative QCD effects may be hard to achieve [27–29]. While the claim of possible LFUV in B meson decays has largely disappeared in the latest LHCb publications [30, 31], the interest in $\bar{b} \to \bar{s}\ell^+\ell^-$ decays in general and in potential LFUV in these processes remains strong [32].

In this paper we describe a search for LFUV in $B^+ \to K^+\ell^+\ell^-$ decays using data collected by the CMS experiment at the LHC in 2018. A special trigger and storage strategy was used to collect a large unbiased sample of $\sim$10 billion b hadron decays. We also report a measurement of the branching fraction of the $B^+ \to K^+\mu^+\mu^-$ decay, both differentially over the dimuon mass squared q^2 and integrated over two different q^2 ranges. The numeric values corresponding to figures and tables in this paper can be found in the HEPDATA database [33].

This paper is organized as follows. After discussing the measurement strategy in section 2, followed by the detector description in section 3, we introduce the data and simulated samples in section 4, and event reconstruction in section 5. We discuss the maximum likelihood fit to the $K^+\ell^+\ell^-$ invariant mass distributions in section 6, followed by the description of the systematic uncertainties in section 7. The results are presented in section 8, followed by the summary of the paper in section 9. Additional plots and details of the $R(K)$ measurement formalism can be found in appendix.

2. Measurement strategy

To maximize the sensitivity to LFUV in $\bar{b} \to \bar{s}\ell^+\ell^-$ decays, it is advantageous to use an observable that minimizes the theoretical uncertainty in its prediction. Given that the absolute $\bar{b} \to \bar{s}\ell^+\ell^-$ rates are poorly understood because of the potentially large long-range corrections [27], a more robust variable is the ratio of muon to electron decays within a certain range of the dilepton mass squared, $q^2_{\min} < q^2 < q^2_{\max}$:

$$R(K)_{\text{theory}}\left[q^2_{\min}, q^2_{\max}\right] = \frac{\mathcal{B}\left(B^+ \to K^+\mu^+\mu^-\right)\left[q^2_{\min}, q^2_{\max}\right]}{\mathcal{B}\left(B^+ \to K^+e^+e^-\right)\left[q^2_{\min}, q^2_{\max}\right]}. \tag{1}$$

This ratio is very close to unity in the SM [34–37] and known to a precision of about 1%. Furthermore, the experimental systematic uncertainties related to signal reconstruction and selection can be reduced by measuring $R(K)$ as a double ratio normalized to the corresponding $B^+ \to J/\psi K^+$ decay channels:

$$R(K)\left(q^2\right)\left[q^2_{\min}, q^2_{\max}\right] = \frac{\left[\frac{\mathcal{B}\left(B^+ \to K^+\mu^+\mu^-\right)\left[q^2_{\min}, q^2_{\max}\right]}{\mathcal{B}(B^+ \to J/\psi(\mu^+\mu^-)K^+)}\right]}{\left[\frac{\mathcal{B}(B^+ \to K^+e^+e^-)\left[q^2_{\min}, q^2_{\max}\right]}{\mathcal{B}(B^+ \to J/\psi(e^+e^-)K^+)}\right]}. \tag{2}$$

This definition of $R(K)$ benefits from the fact that the branching fractions $\mathcal{B}(J/\psi \to \mu^+\mu^-)$ and $\mathcal{B}(J/\psi \to e^+e^-)$ are measured to be the same within a precision of about 0.7% [4], which ensures that this extra normalization does not change the value of $R(K)$ with respect to the definition in

equation (1). Additionally, since the leptons from the nonresonant $B^+ \to K^+\ell^+\ell^-$ and the resonant $B^+ \to J/\psi(\ell^+\ell^-)K^+$ decays occupy a similar phase space, with a similar acceptance and efficiency after the final selection, most of the systematic uncertainties related to the lepton momentum scale and identification cancel in equation (2), making it an excellent experimental observable directly related to $R(K)_{\text{theory}}$.

The $R(K)$ ratio in equation (2) is measured in the q^2 region from 1.1 to 6.0 GeV^2, referred to as the 'low-q^2' region, which is free of dilepton resonances. This choice is optimized to exclude the contributions of the $\phi(1020)$ and lighter resonances at the lower end of the q^2 spectrum, and the tail of the J/ψ resonance at the higher end. In addition, the chosen lower boundary reduces the kinematic difference between the muon and electron decay channels due to the differences in their masses.

For the differential branching fraction measurement in the $B^+ \to K^+\mu^+\mu^-$ channel, the q^2 range is extended downward by adding a $q^2 < 0.98\,\text{GeV}^2$ bin, below the $\phi(1020)$ resonance, and upward by introducing nine bins up to the kinematic limit of $q^2 = 22.9\,\text{GeV}^2$, excluding the J/ψ and $\psi(2S)$ resonance q^2 ranges. Furthermore, the low-q^2 region is split into five finer bins. The definition of the 15 q^2 bins used for the differential measurement is given in section 8 (table 10). The chosen binning ensures a sufficient number of events per bin to reliably extract the branching fraction of the $B^+ \to K^+\mu^+\mu^-$ decay and is similar to that used in the LHCb analysis [24], which presently dominates the precision of these differential branching fraction measurements [4].

In addition to the low-q^2 region, part of which is defined as the signal region (SR) as described in section 5, two control regions (CRs) are defined based on the dilepton q^2, as follows.

- J/ψ CR: the $8.41 < q^2 < 10.24\,\text{GeV}^2$ range is used for the $B^+ \to J/\psi(\ell^+\ell^-)K^+$ decay, which is the main normalization channel used in the $R(K)$ measurement.
- $\psi(2S)$ CR: the $12.6 < q^2 < 14.44\,\text{GeV}^2$ range is used for the $B^+ \to \psi(2S)(\ell^+\ell^-)K^+$ decay, which is the secondary normalization channel, used as an additional cross-check, with the $R_{\psi(2S)}$ ratio defined as:

$$R_{\psi(2S)} = \frac{\left[\frac{\mathcal{B}\left(B^+\to\psi(2S)\left(\mu^+\mu^-\right)K^+\right)}{\mathcal{B}(B^+\to J/\psi(\mu^+\mu^-)K^+)}\right]}{\left[\frac{\mathcal{B}(B^+\to\psi(2S)(e^+e^-)K^+)}{\mathcal{B}(B^+\to J/\psi(e^+e^-)K^+)}\right]}. \tag{3}$$

  This ratio is very close to unity in the SM and has been measured to a precision of about 8%, with the uncertainty dominated by the current precision of the measurement of the $\psi(2S) \to \mu^+\mu^-$ branching fraction [4].

The analysis is conducted using the 'data blinding' concept [38]. In the muon channel, a random scale factor (SF) is initially applied to the nonresonant signal yields in each q^2 bin. In the electron channel, the $K^+e^+e^-$ invariant mass spectrum in the vicinity of the B^+ peak in the low-q^2 region is initially kept blind. The entire analysis is optimized using simulated samples and resonant CRs, and the unblinding of the data in both channels is done only as the final step.

3. The CMS detector

The central feature of the CMS apparatus is a superconducting solenoid of 6 m internal diameter, providing a magnetic field of 3.8 T. Within the solenoid volume are a silicon pixel and strip tracker, a lead tungstate crystal electromagnetic calorimeter (ECAL), and a brass and scintillator hadron calorimeter, each composed of a barrel and two endcap sections. Forward calorimeters extend the pseudorapidity (η) coverage provided by the barrel and endcap detectors. The ECAL consists of 75 848 lead tungstate crystals, which provide coverage in a barrel region, $|\eta| < 1.48$, and two endcap regions, $1.48 < |\eta| < 3.0$. Muons are measured in gas-ionization detectors embedded in the steel flux-return yoke outside the solenoid. The procedure followed for aligning the detector is described in [39].

The silicon tracker measures charged particles within the range $|\eta| < 3.0$. During the 2018 LHC running period, when the data used in this paper were recorded, the silicon tracker consisted of 1856 silicon pixel [40] and 15 148 silicon strip detector modules. For nonisolated particles with transverse momentum in the $1 < p_T < 10\,\text{GeV}$ range, the track resolutions are typically 1.5% in p_T and 20–75 μm in the transverse impact parameter [41]. Muons are measured in the $|\eta| < 2.4$ range, with detection planes made using three technologies: drift tubes, cathode strip chambers, and resistive-plate chambers. Matching muons to tracks measured in the silicon tracker results in a relative transverse momentum resolution, for muons with p_T up to 100 GeV, of 1% in the barrel and 3% in the endcaps [42]. The efficiency to reconstruct and identify muons is greater than 96%. The electron momentum is estimated by combining the energy measurement in the ECAL with the momentum measurement in the tracker. The momentum resolution is typically better than 5% for electrons in the range $1 < p_T < 10\,\text{GeV}$. It is generally better in the barrel region than in the endcaps, and also depends on the bremsstrahlung energy emitted by the electron as it traverses the material in front of the ECAL [43–46].

Events of interest are selected using a two-tiered trigger system. The first level (L1), composed of custom hardware processors, uses information from the calorimeters and muon detectors to select events at a rate of around 100 kHz within a fixed latency of 4 μs [47]. The second level, known as the high-level trigger (HLT), consists of a farm of processors running a version of the full event reconstruction software optimized for fast processing, and further reduces the event rate before data storage [48].

A more detailed description of the CMS detector, together with a definition of the coordinate system used and the relevant kinematic variables, can be found in [49].

Table 1. Summary of the loosest muon trigger requirements imposed by the L1 and HLT algorithms for each instantaneous luminosity scenario: the L1 and HLT muon transverse momentum thresholds p_{T}^{μ}, and the HLT muon impact parameter significance $\mathrm{IP_{sig}}$. Also shown are the trigger purity, peak HLT rate, and $\int \mathcal{L}\mathrm{d}t$. The second trigger was the highest threshold one during early data taking, corresponding to $\int \mathcal{L}\mathrm{d}t = 6.9\,\mathrm{fb}^{-1}$, and then the second-highest for the rest of the data taking, accumulating $\int \mathcal{L}\mathrm{d}t = 26.7\,\mathrm{fb}^{-1}$ out of $34.7\,\mathrm{fb}^{-1}$ collected by the highest threshold trigger.

$\mathcal{L}$ (10^{34} cm^{-2} s^{-1})	L1 p_{T}^{μ} thr. (GeV)	HLT p_{T}^{μ} thr. (GeV)	HLT μ $\mathrm{IP_{sig}}$ thr.	Purity (%)	Peak HLT rate [kHz]	$\int \mathcal{L}\mathrm{d}t$ [fb^{-1}]
1.7	12	12	6	92	1.5	34.7
1.5	10	9	6	87	2.8	6.9 + 26.7
1.3	9	9	5	86	3.0	20.9
1.1	8	8	5	83	3.7	8.3
0.9	7	7	4	59	5.4	6.9

4. Data and simulated samples

4.1. B parking data sample

For the purpose of this analysis, we deployed a novel trigger and data processing strategy in CMS during the 2018 data-taking period at the proton-proton (pp) center-of-mass energy of 13 TeV, referred to as 'B parking'. This strategy enabled the collection of order 10^{10} unbiased b hadron decays [44, 45] by exploiting the fact that b hadrons are predominately produced in pairs, and therefore one can trigger on one b hadron of the pair using a specific decay mode ('tag-side' b hadron), while the other b hadron ('probe-side' b hadron) decay is *unbiased* by the trigger.

The trigger strategy relies on tag-side final states that include a muon with a relatively high p_{T} and a significant displacement from the pp collision point. This strategy is motivated by the significant fraction (nearly 40%) of $\mathrm{b\bar{b}}$ events that include at least one muon from a b hadron (or subsequent charm hadron) decay, combined with the relatively low rate of L1 single-muon triggers. In addition, the B parking strategy takes advantage of the gradual decrease of the L1 trigger rate and online computing resources use by the nominal CMS physics program as the instantaneous luminosity $\mathcal{L}$ decreases during each LHC fill. To exploit the available L1 (HLT) bandwidth of up to 30 (5.4) kHz, the B parking trigger requirements were gradually relaxed during each LHC fill. This strategy does not affect the main, high-p_{T} physics program of CMS, while offering a significant increase in the CMS potential in flavor physics, including the present $R(\mathrm{K})$ measurement.

Table 1 summarizes the B parking muon trigger requirements imposed by the L1 and HLT algorithms. The L1 trigger logic requires the presence of a muon with $|\eta| < 1.5$ and with a variable minimum p_{T} threshold. These requirements help to control the L1 rate by removing events with muons at low p_{T} and large $|\eta|$, which are dominated by those produced in pileup interactions (additional minimum bias interactions within the same or adjacent bunch crossings). In addition, a single-muon L1 trigger with $p_{\mathrm{T}} > 22\,\mathrm{GeV}$ in the full pseudorapidity range $|\eta| < 2.4$ is used. Since the muon displacement information is not available at L1, only p_{T} and $|\eta|$ thresholds are used to control the rate. At the HLT, the p_{T} threshold is sharpened, given the more precise momentum reconstruction compared to that at L1, and a minimum requirement is imposed on the two-dimensional (2D) muon track impact parameter significance $\mathrm{IP_{sig}}$, defined as the distance of closest approach of the track to the beam line (the measured line of the proton beams inside the CMS detector [50]), divided by its uncertainty. These triggers are 'nested', i.e. the most restrictive trigger is exposed to the largest integrated luminosity ($\int \mathcal{L}\mathrm{d}t$), while the looser ones have progressively higher efficiency but lower $\int \mathcal{L}\mathrm{d}t$.

The purity of the B parking sample is defined as the fraction of triggered events containing a b hadron decay and is evaluated by counting the number of $\mathrm{B^0} \to \mathrm{D^{*+}}\mu^-\overline{\nu}_\mu \to \mathrm{D^0}\pi^+_{\mathrm{soft}}\mu^-\overline{\nu}_\mu \to \mathrm{K^-}\pi^+\pi^+_{\mathrm{soft}}\mu^-\overline{\nu}_\mu$ events, using the known $\mathrm{B^0}$ meson production fraction f_{d} and the relevant branching fractions [4]. For the π^+_{soft}, the p_{T} threshold is set at 0.5 GeV. The purity is measured both in data and in simulation (described in section 4.2), with good agreement between the two estimates. The purity ranges between 59% and 92%, depending on the trigger thresholds, with an average of ≈80% in the collected data set.

The B parking data set corresponds to $\int \mathcal{L}\mathrm{d}t = 41.6 \pm 1.0\,\mathrm{fb}^{-1}$ [51], about 30% less than the $\int \mathcal{L}\mathrm{d}t$ of 59.8 fb^{-1} collected with the main physics triggers operating during the entire 2018 data taking. It took about a year to fully reconstruct these data during the LHC Long Shutdown 2; hence the name: B parking.

4.2. Event simulation

Monte Carlo (MC) simulated samples are used to optimize the analysis and model various background sources. Signal and background processes are generated with PYTHIA 8.230 [52], including parton showering, fragmentation, and hadronization. The PYTHIA output is interfaced with EVTGEN 1.3.0 [53], which simulates various b hadron decays. The underlying event is also modeled with PYTHIA, using the CP5 tune [54]. The parton distribution functions (PDFs) are taken from the NNPDF3.1 set [55]. Final-state photon radiation is modeled with PHOTOS 3.61 [56]. The $\mathrm{B^+} \to \mathrm{K^+}\ell^+\ell^-$ signal is generated with the BTOSLLBALL, setting 6, model of the EVTGEN decay library, based on form-factors from [57]. While more precise form-factor determinations are now available both from light-cone sum

rules [58, 59] and lattice QCD [60], we do not expect them to have a significant impact on the decay kinematics. Additionally, the following processes are simulated: the $B^+ \to J/\psi K^+$ and $B^+ \to \psi(2S)K^+$ resonant decays, and $B^0 \to J/\psi K^*(892)^0$, $B^0 \to \psi(2S)K^*(892)^0$, $B^0 \to K^*(892)^0\ell^+\ell^-$, $B^+ \to J/\psi K^*(892)^+$, $B^+ \to \psi(2S)K^*(892)^+$, and $B^+ \to K^*(892)^+\ell^+\ell^-$ backgrounds, as well as inclusive b hadron samples, and Cabibbo-suppressed $B^+ \to J/\psi\,\pi^+$, $B^+ \to \psi(2S)\pi^+$, and $B^+ \to \pi^+\ell^+\ell^-$ decays, with and without emulation of the trigger requirements. The CMS detector response is simulated using GEANT4 [61]. All MC samples are reconstructed with the same software packages as used for collision data and include effects of pileup by overlaying simulated minimum bias events on the hard-scattering event, with the multiplicity distribution matching that in data.

5. Event reconstruction and selection

The particle-flow (PF) algorithm [62] aims to reconstruct and identify each individual particle (muon, electron, photon, and charged and neutral hadrons) in an event, with an optimized combination of information from the various elements of the CMS detector.

Muons are identified as tracks in the silicon tracker consistent with either a track or several hits in the muon system, and associated with calorimeter deposits compatible with the muon hypothesis [42]. A muon that triggered the event readout is required to pass the 'medium' muon identification criteria of [42]. As multiple pp collision vertices are reconstructed from each beam crossing, we select a single primary vertex (PV) as the one whose z position is closest to that of the point of closest approach of this muon to the beam line. In addition, for the electron channel, only electron candidates consistent with originating from this PV are considered. This procedure significantly reduces the contamination from pileup interactions. To simplify the trigger efficiency calculations, the muon channel analysis uses only one HLT path, which requires a muon with $p_T > 9\,\text{GeV}$ and $\text{IP}_{\text{sig}} > 6$. This trigger was the highest threshold one during early B parking data taking, corresponding to $\int \mathcal{L}dt = 6.9\,\text{fb}^{-1}$, and then the second-highest for the rest of the data taking, accumulating an additional $\int \mathcal{L}dt = 26.7\,\text{fb}^{-1}$. Therefore, the $\int \mathcal{L}dt$ used for the muon channel is $33.6\,\text{fb}^{-1}$, as shown in the second row of table 1.

The PF algorithm used for electron reconstruction imposes an implicit minimum electron p_T requirement of 2 GeV. To recover the efficiency loss for low-p_T (LP) electrons, an additional algorithm ('LP electron reconstruction') was specifically developed. As is the case for the PF algorithm, in the LP algorithm, the determination of the charged-particle track parameters for electron candidates, in the presence of bremsstrahlung energy loss, relies on the use of a Gaussian sum filter [43]. The LP electron candidate reconstruction is started with a combination of two boosted decision trees (BDTs), which are trained on samples of low-p_T electrons and result in looser reconstruction requirements than for the PF electrons. The LP electrons in this analysis are reconstructed down to 1 GeV, which ensures that they reach the ECAL. In case of duplicates, we preferentially select PF electrons over LP ones. To optimize the performance of the electron identification, several electron candidate characteristics are combined using a BDT into a single discriminating variable, referred to as ID, analogously to what was done in [43]. The ID BDTs are trained separately for PF and LP electrons. The PF electron ID BDTs were retrained specifically for this analysis to improve the performance at low p_T. The training was done separately for two ranges, $2 < p_T < 5\,\text{GeV}$ and $p_T > 5\,\text{GeV}$, while a single training is used for the LP electron ID in the entire p_T range. The input variables for the ID BDTs include both track-related quantities and calorimetric shower shapes, as well as variables related to the matching of the extrapolated track to the calorimeter cluster and the difference between the track momentum at the innermost and outermost tracker layers. The electron ID BDTs were trained with the XGBOOST algorithm [63] on a simulated sample of $B^+ \to J/\psi(e^+e^-)K^+$ events. The electron p_T and η distributions of the training sample have been reweighted to reproduce those for the background, to avoid biases. The 'tag-and-probe' method [64] using $J/\psi \to e^+e^-$ decays in data is used to check the accuracy of the simulation for the ID BDT input variables, as well as for the output distribution. We find these variables for both the PF and LP electrons in data to be consistent with those in simulation, within statistical uncertainties.

To measure $R(K)$, we select events for which either a $B^+ \to K^+\mu^+\mu^-$ candidate (used in the numerator of the $R(K)$ ratio) is found on the tag side, i.e. a muon from the $B^+ \to K^+\mu^+\mu^-$ candidate must satisfy the trigger conditions, or a $B^+ \to K^+e^+e^-$ candidate (used in the denominator of the $R(K)$ ratio) is found on the probe side. While using the tag side for the muon channel and probe side for the electron channel complicates the analysis, as the trigger efficiency does not cancel in the $R(K)$ ratio, this choice ensures a large number of events collected in the $B^+ \to K^+\mu^+\mu^-$ channel and not only maximizes the sensitivity of the $R(K)$ measurement, but also enables high-precision measurements of the $B^+ \to K^+\mu^+\mu^-$ branching fraction.

The B^+ candidates are formed using a pair of opposite-sign (OS) same-flavor leptons with an invariant mass below 5 GeV and a positively charged track, to which the kaon mass is assigned. Several quality criteria are applied to each muon, electron, and track candidates to reduce the number of misreconstructed objects. Specifically, tracks are required to pass the 'high-purity' track quality criteria [62, 65] with $p_T > 1\,\text{GeV}$ and $|\eta| < 2.4$. Since the triggering object is a muon, to reconstruct the $B^+ \to K^+\mu^+\mu^-$ decay only one additional muon is needed. This muon is required to have OS with respect to the triggering muon, pass the 'medium' muon identification criteria, have $p_T > 2\,\text{GeV}$, and satisfy $|\eta| < 2.4$. In the electron channel, in order to increase the purity of the sample, we require at least one of the electrons to be reconstructed with the PF algorithm. Both electrons are required to have $|\eta| < 2.4$. The two electrons must have points of origin separated, along the beam line direction, by $|\Delta z| < 1\,\text{cm}$ and with $|\Delta z| < 1\,\text{cm}$ of the point of origin of the muon that triggered the event. At this stage, we apply only very loose requirements

Table 2. Input variables used in the muon and electron channel BDTs.

Variable	Description
	Common variables
$\cos\alpha_{2D}(B^+)$	Cosine of the angle in the plane transverse to the beams between the momentum vector of the B^+ candidate and the line connecting the beam line and the SV.
$p(B^+ \text{ vtx})$	Probability of the SV kinematic fit.
L_{xy}/σ_{xy}	Significance of the SV displacement in the transverse plane with respect to the beam line.
$p_T(B^+)$	Transverse momentum of the B^+ candidate; in the electron channel it is divided by $m_{K^+e^+e^-}$.
$p_T(K^+)$	Transverse momentum of the K^+ candidate; in the electron channel it is divided by $m_{K^+e^+e^-}$.
	Muon channel variables
$\min\Delta R(\mu, K^+)$	$\Delta R = \sqrt{(\Delta\eta)^2 + (\Delta\phi)^2}$ distance between the K^+ candidate and the closest muon candidate.
$\min\Delta z(\mu, K^+)$	Δz distance between the points of origin of the K^+ candidate and the closest muon candidate along the beam line direction.
$\text{Iso}(\mu_{\text{lead}})$	PF isolation for the p_T-leading muon candidate, defined as a scalar p_T sum all PF candidates, excluding the muon candidate itself, within $\Delta R < 0.4$ of the muon candidate and corrected for pileup.
	Electron channel variables
$p_T(P_i)/m_{K^+e^+e^-}, i = 1,2$	Transverse momenta of the two electron candidates, divided by $m_{K^+e^+e^-}$.
$\Delta z(P_i, K^+),\ i = 1,2$	Longitudinal distance between the points of origin of each electron candidate and the kaon candidate.
$\frac{\lvert d_{3D}(K^+, e^+e^-)\rvert}{\sigma_{\lvert d_{3D}(K^+, e^+e^-)\rvert}}$	Kaon candidate 3D impact parameter significance with respect to the dielectron vertex.
$\Delta R(e^+, e^-)$	ΔR between the two electron candidates.
$\Delta R(P_i, K^+),\ i = 1,2$	ΔR between each electron candidate and the kaon candidate.
$\frac{\lvert\mathbf{p}(e^+e^-)\times\mathbf{r}\rvert - \lvert\mathbf{p}(K^+)\times\mathbf{r}\rvert}{\lvert\mathbf{p}(e^+e^-)\times\mathbf{r}\rvert + \lvert\mathbf{p}(K^+)\times\mathbf{r}\rvert}$	Asymmetry of the momentum of the dielectron system and that of the K^+ momentum with respect to the B^+ candidate trajectory, where $\mathbf{r}$ is a unit vector connecting the PV and SV.
$\text{ID}(P_i,\ i = 1,2)$	Electron ID BDT score for two electron candidates.
$I^{\text{rel}}_{\Delta R=0.4}(P_i),\ i = 1,2$ and $I^{\text{rel}}_{\Delta R=0.4}(K^+)$	Relative track-based isolation of the two electron candidates and the K^+ candidate, respectively, defined as a scalar p_T sum of all additional tracks in a $\Delta R < 0.4$ cone around the candidate, divided by the candidate's p_T.

on the ID BDT output for the electrons, as it is used as an input to the multivariate analysis described below. The transverse momentum of the B^+ candidate is required to exceed 3 and 1.75 GeV in the muon and electron channels, respectively.

The tracks of the three particles forming the B^+ candidate are fitted to a common vertex, using their measured momentum vectors with the corresponding uncertainties, to improve the mass measurement accuracy for both the B^+ candidate and the lepton pair. The kinematic fit algorithm [66] constrains the tracks belonging to the B^+ candidates to originate from a single vertex, and provides the vertex position, covariance matrix, and χ^2 of the fit. After the vertexing is performed, the particle trajectories are refitted using this secondary vertex (SV) as an additional constraint, and their momenta are recomputed. The masses of the particles (leptons and kaon) are fixed to their nominal values [4]. A loose set of criteria is imposed on the SV fit probability, as well as the L_{xy}/σ_{xy} and $\cos\alpha_{2D}(B^+)$ variables described in table 2. The invariant mass of the B^+ candidate is required to be in the range 5.0–5.6 (4.7–5.7) GeV for the muon (electron) channel. In addition, in the electron channel, the two electron candidates are fitted to a common vertex ('dielectron vertex'), which is used later in the analysis to define one of the discriminating variables, $|d_{3D}(K^+, e^+e^-)|$, described in table 2.

A significant fraction of semileptonic decays of heavy-flavor hadrons, containing a semileptonic charm meson decay or a hadronic $D^0 \to K^-\pi^+$ decay, remains in the preselected sample. The hadronic D^0 decays enter the sample because of misidentification of the K^- or π^+ meson as a lepton. Therefore, a charm veto is applied by requiring that, for a B^+ candidate, the invariant mass of the track, using the pion mass assignment, and the OS lepton, using the kaon mass assignment, is larger than 2 GeV. In the electron channel, we additionally require the invariant mass of the track, using the kaon mass assignment, and the OS electron, using the pion mass assignment, to also be larger than 2 GeV. This additional selection is not applied in the muon channel, as the probability to reconstruct charged pions as muons is significantly smaller

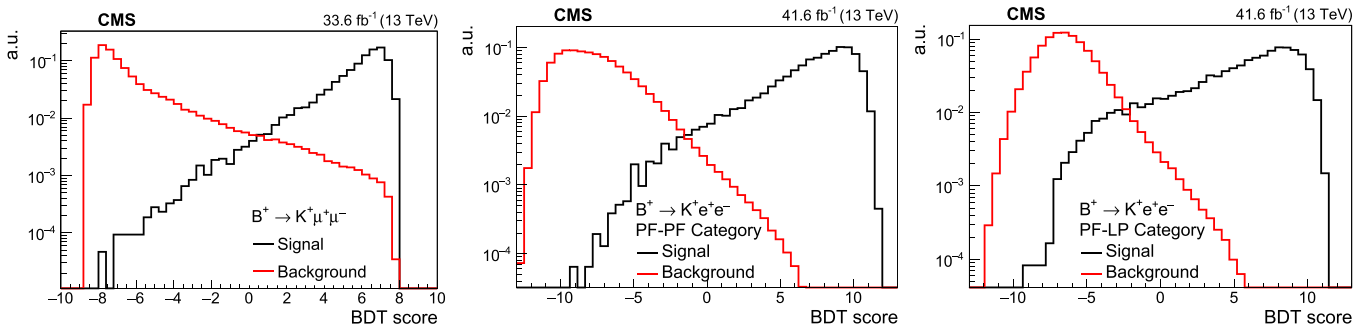

Figure 2. Analysis BDT output for signal (MC simulation, in black) and background (same-sign dilepton data, in red) for the muon channel (left) and for the PF-PF (center) and PF-LP (right) electron channels. The histograms are normalized to unit area.

than that for kaons. Finally, to suppress events where a muon is misreconstructed as a kaon candidate, the track under the muon mass hypothesis and the OS muon belonging to a B^+ candidate are required to have an invariant mass away from known dimuon resonances.

The selected B^+ candidates are binned in q^2, as described in section 2. Events in each q^2 bin can be further divided in regions based on the invariant mass of the B^+ candidate. The region where genuine B^+ candidates are expected, $5.07 < m_{K^+\ell\ell} < 5.49\,\text{GeV}$, is denoted as the SR. The adjacent mass regions $4.90 < m_{K^+\mu^+\mu^-} < 5.07$ $(4.91 < m_{K^+e^+e^-} < 5.07)\,\text{GeV}$ and $5.49 < m_{K^+\ell\ell} < 5.65\,\text{GeV}$ are designated as sidebands (SBs). The low-mass SB has a significant contamination from partially reconstructed B meson decays, while the high-mass SB is dominated by combinatorial background.

The final selection in each channel is based on a BDT, which combines several variables into a classifier built using the XGBoost package. The input variables used in the BDT are selected based on the forward elimination method (i.e. by adding one variable at a time and either keeping or dropping it based on the observed improvement in the performance) and are summarized in table 2. In the electron channel, two independent BDTs are trained for the PF-PF and PF-LP categories using the same input variables. Given the significantly higher background in the electron channel, the corresponding BDTs have more input variables and have all the momenta variables normalized to the B^+ candidate mass $m_{K^+e^+e^-}$ to ensure that a BDT score selection does not introduce peaks in the invariant mass distributions ('mass sculpting'). Both muon and electron BDTs are tested thoroughly using data and simulated events to ensure that they do not introduce any mass sculpting. The BDTs are trained in a supervised manner with simulated $B^+ \to K^+\ell^+\ell^-$ decays in the low-q^2 bin as signal and data events from the low-q^2 bin SBs as background.

It is checked that the simulation describes the data well. The comparisons are performed for all BDT input variables, as well as the BDT output, using the ${}_s\mathcal{P}$lot technique [67], where the reconstructed B^+ candidate invariant mass is used as the discriminating variable. The test is performed on the $B^+ \to J/\psi(\ell^+\ell^-)K^+$ CRs, and good agreement between data and simulation is found for all three channels (muon, PF-PF, and PF-LP). After training, the BDT output is a continuous function, as shown in figure 2, where high (low) values correspond to signal-like (background-like) events. In this figure, the background sample is obtained by using the SR selection, with the inversion of the OS requirement for the two leptons (the same-sign CR). The optimal BDT working point (WP) is chosen to maximize the expected significance of the $B^+ \to K^+\ell^+\ell^-$ signal in the low-q^2 region. In the muon channel, the same BDT selection is applied to the J/ψ and $\psi(2S)$ CRs to allow for maximum cancellation of the systematic uncertainties, while in the electron channel, where the dominant uncertainty is statistical, a looser BDT WP is used for the resonance CRs to maximize the number of events in the normalization channel. The muon, PF-PF, and PF-LP channels are then combined statistically for the $R(K)$ extraction.

The product of the detector acceptance $\mathcal{A}$ and efficiency ϵ is evaluated using simulated samples without the trigger requirements. For the muon channel, the trigger efficiency ϵ_{trig}, determined from simulated samples with and without the trigger requirement and no reconstruction requirements, is found to be approximately 0.4%. The low value of the trigger efficiency is mainly due to the muon p_T and displacement requirements. In the electron channel, since the $B^+ \to K^+e^+e^-$ candidates are found on the probe side, the ϵ_{trig} component does not enter in the $R(K)$ extraction, as it is measured to be the same for the low-q^2 and the J/ψ regions and hence cancels completely in the $R(K)$ ratio.

Slight differences between data and simulation in the muon channel are mitigated with SFs applied to simulated events, and the correction for the following effects are applied.

- Trigger efficiency: the difference in the trigger response is corrected for by an SF, as a function of muon η, p_T, and the SV displacement significance L_{xy}/σ_{xy}. The SF is measured with a tag-and-probe method [64], exploiting the $J/\psi \to \mu^+\mu^-$ decays.
- Muon identification efficiency: the quality criteria imposed on the muons may have different performance in data and simulation. This SF is measured with the tag-and-probe method.
- BDT efficiency: the BDT is using input variables that have small differences between data and simulation. The

Table 3. The product of acceptance, and offline and trigger efficiency ($\mathcal{A}\epsilon\epsilon_{\text{trig}}$) for the signal in the low-q^2 region and for the two resonance CRs. In the case of electrons, the trigger efficiency is not included in the quoted $\mathcal{A}\epsilon$ numbers, as it cancels out in the $R(\text{K})$ double ratio. Uncertainties are statistical only.

q^2 range	Muon $\mathcal{A}\epsilon\epsilon_{\text{trig}}$ (%)	PF-PF $\mathcal{A}\epsilon$ (%)	PF-LP $\mathcal{A}\epsilon$ (%)
Low q^2	0.0825 ± 0.0013	2.95 ± 0.07	1.50 ± 0.05
J/ψ	0.0969 ± 0.0006	2.48 ± 0.03	1.08 ± 0.01
ψ(2S)	0.1112 ± 0.0004	1.82 ± 0.02	0.68 ± 0.01

corresponding SF is measured by comparing the BDT output for the $\text{B}^+ \to \text{J}/\psi(\mu^+\mu^-)\text{K}^+$ events in data and simulation.
- Pileup: simulated events are reweighted to match the evolving pileup conditions of the analyzed data.
- Higher-order corrections: leading-order PYTHIA simulation is reweighted at the generator-level so that the B meson p_{T} and rapidity spectra match those from fixed-order perturbative quantum chromodynamics calculations with resummation of large logarithms that arise from soft and collinear emissions [68, 69]. The reweighting is done using the fixed-order plus next-to-leading logarithmic (FONLL) calculations [70, 71], which are known to reproduce these spectra in data with high accuracy.

It was found that applying the analogous SFs to the electron channel changes the measured value of $R(\text{K})$ by less than 1.2%, which has a negligible effect on the final result given the large statistical uncertainty in the electron channel. Therefore, the SFs are not applied in the electron channel. The measured $\mathcal{A}\epsilon\epsilon_{\text{trig}}$ in the muon channel for all q^2 bins, after applying these corrections, is shown in figure A1. The $\mathcal{A}\epsilon\epsilon_{\text{trig}}$ or $\mathcal{A}\epsilon$ values in the low-q^2 regions and two resonant CRs for the muon or electron channel are listed in table 3.

6. Mass fit

In each channel, the $\text{B}^+ \to \text{K}^+\ell^+\ell^-$ signal yield is extracted from an unbinned maximum likelihood fit to the invariant mass spectrum of all B^+ candidates that pass the selection criteria. Signal and background shapes are described by analytical functions or templates based on studies of simulated events, with their normalization factors free to vary in the fit to data. To allow a better description of the data, some parameters of the analytical functions are constrained within the uncertainties obtained from a fit to simulated samples, rather than being fixed. The same functional forms describing the various contributions are shown to work well in all q^2 bins in simulation; hence they are kept the same in the fit to data as well.

6.1. Background composition

While the background composition differs from one q^2 bin to another and from channel to channel, the background originates from the following common sources:

- Combinatorial background: this background stems from the combination of objects from different b hadron decays, or two muons from the same b hadron decay chain, with a random track. The shape is extracted by exploiting the fact that this background dominates the upper B^+ mass SB, as well as the same-sign CR.
- Partially reconstructed background: this background is dominated by the $\text{B}^{*0/+} \to \text{K}^*(892)^{0/+}\text{X}$ decays, where X is J/ψ, ψ(2S), or a nonresonant $\ell^+\ell^-$ pair. This background arises from $\text{K}^*(892)^0 \to \text{K}^+\pi^-$, $\text{K}^*(892)^+ \to \text{K}^+\pi^0$, and $\text{K}^*(892)^+ \to \text{K}^0\pi^+$ decays, where either the K^+ or π^+ track is used together with the dilepton system to build a B^+ candidate, with the other decay particle being either lost or ignored. In the latter case, potentially two B^+ candidates are reconstructed by combining the dilepton system with either of the two tracks; both have significantly lower mass than the nominal B^+ meson mass due to the missing other particle, but still potentially contaminate the signal window in the $\text{K}\ell^+\ell^-$ mass. Simulated $\text{B}^{*0/+} \to \text{K}^*(892)^{0/+}\text{X}$ events are used to derive the invariant mass distributions of the partially reconstructed backgrounds.
- Cabibbo-suppressed background: this background is present in both the resonant CRs and nonresonant SR, and it is very similar to the signal signature, just with the kaon replaced by a pion. This background cannot be discriminated from the signal decay and it is accounted for using simulated events.
- Resonant background 'leakage': this background comes from the fact that leptons produced in the $\text{B}^+ \to \text{J}/\psi(\ell^+\ell^-)\text{K}^+$ and $\text{B}^+ \to \psi(2\text{S})(\ell^+\ell^-)\text{K}^+$ decays can radiate final-state photons. In the case of muons, no photon recovery algorithm is used, so these photons are not accounted for in the muon momentum reconstruction; in the case of electrons, while most of these photons are picked by the Gaussian sum filter algorithm and added to the momentum of the reconstructed electrons, large-angle radiation may still be missed. These effects reduce the q^2 to lower values and generally result in migration of events across the q^2 bins. The finite detector resolution and a much larger branching fraction to the resonant mode can also contribute tails on the high side. This background source is significant only in the q^2 bins in the vicinity of the J/ψ and ψ(2S) resonances, and is estimated using simulated samples.
- Other b hadron decays: this is the most general background that includes all partially reconstructed b hadron decays that do not fit in any of the previous categories. Depending on the q^2 bin, different specific decays dominate in this category. The shape of this background was evaluated using an inclusive sample of soft QCD processes generated with PYTHIA, with a filter that selected b hadron production. The $m_{\text{K}^+\ell\ell}$ distribution in this sample was found to be well described by a falling exponential function in all q^2 bins.

A potential peaking background in the electron channel could arise from hadrons misidentified as electrons in the all-hadronic decays of the type $\text{B}^+ \to \text{K}^+\text{h}_1\text{h}_2$, where $\text{h}_{1,2}$ are hadrons, dominated by $\text{B}^+ \to \text{K}^+\pi^+\pi^-$ decays (with the

branching fraction of $\sim 10^{-5}$, once the resonant charm $\overline{\mathrm{D}}^0\pi^+$ contribution is subtracted). The peaking structure is particularly pronounced in the low-q^2 region where the dipion system generally has large momentum, and replacing it with the dielectron hypothesis consequently does not shift sizably the reconstructed invariant mass. This background, missed in early $R(\mathrm{K})$ measurements [9, 19, 20], was largely responsible for the claimed anomaly, and after accounting for it, the $R(\mathrm{K})$ value is found to be compatible with the SM expectation [30, 31]. In the present analysis, we have developed the identification of low-p_T electrons and optimized the identification of PF electrons specifically to reduce the probability of such misidentification. A typical misidentification rate after the BDT selection is 10^{-3}–10^{-4} per electron, making the misidentified-hadron background very small. Nevertheless, given the importance of the peaking background in the LHCb case, we have made an explicit estimate of potential contributions of the misidentified-hadron background. We use a large simulated sample of $\mathrm{B}^+ \to \overline{\mathrm{D}}^0(\to \mathrm{K}^+\pi^-)\pi^+$ decays without applying the charm veto (described in section 5) to estimate the misidentification efficiency. In addition, we use a small simulated sample of charmless $\mathrm{B}^+ \to \mathrm{K}^+\pi^-\pi^+$ decays to evaluate the charm veto efficiency for this mode. The study showed that the charm veto plus the identification requirements on PF and LP electrons work very well to suppress the misidentification background to a low level, as expected from squaring the misidentification probability and applying the relative branching fractions for the signal and background processes. The total estimated number of misidentified-hadron background events in the low-q^2 region after the full analysis selection is less than 0.3 events in each of the PF-PF and PF-LP categories. Compared to the expected signal yield, this peaking background corresponds to <2 and $<6\%$, respectively, for the two categories, which is much smaller than the corresponding statistical uncertainty. As this background is also shown to be negligible in the muon channel, it is not included in the final results.

6.2. Muon channel signal extraction

In the muon channel, two independent unbinned maximum likelihood fits are performed to the B^+ candidate invariant mass distribution: a 'single' fit in the low-q^2 region and a 'simultaneous' fit across the 15 q^2 bins. The former is used to measure $R(\mathrm{K})$ and the integrated branching fraction of the $\mathrm{B}^+ \to \mathrm{K}^+\mu^+\mu^-$ decay, while the latter is used for the extraction of the differential branching fraction. While the two fits give consistent results in the low-q^2 region, both in terms of the central value and the uncertainty, the strategy of having two fits achieves greater similarity between the $\mathrm{B}^+ \to \mathrm{K}^+\mu^+\mu^-$ and $\mathrm{B}^+ \to \mathrm{K}^+\mathrm{e}^+\mathrm{e}^-$ channels and reduces the $R(\mathrm{K})$ measurement uncertainty.

In both the single fit of the low-q^2 region and the simultaneous fit, the signal is described with the sum of a double-sided crystal ball (DCB) function [72, 73] and a Gaussian function. All of the parameters of the DCB function are fixed based on simulation. The mean and the width of the Gaussian function in the single fit are free parameters. In the simultaneous fit, while the width is allowed to float, the mean of the Gaussian function is parameterized as a linear function of q^2 with a slope of $0.0014 \pm 0.0012\,\mathrm{GeV}^{-1}$ to describe the observed dependence in simulation. The rest of the parameters in the simultaneous fit are treated the same way as in the single fit.

- The $\mathrm{B}^+ \to \mathrm{K}^*(892)^{0/+}\mathrm{X}$ background is described by a DCB function with the shape fixed from simulation. In the simultaneous fit, an exponential function with parameters fixed from simulation is added to the DCB function to account for the B^+ candidates built with the π of the $\mathrm{K}^*(892)$ decay in the 11.0–19.24 GeV^2 q^2 range where the contribution of this component is significant.
- The sum of the combinatorial and other B^+ meson decays backgrounds is described with a single exponential function, except for the last q^2 bin of the simultaneous fit, where it is multiplied by $m_{\mathrm{K}^+\mu^+\mu^-} - m_{\mu^+\mu^-} - m_\mathrm{K}^+$ to account for the phase space suppression.
- The $\mathrm{B}^+ \to \pi^+\mathrm{X}$ background is described by a DCB function with the shape and relative yield with respect to the $\mathrm{B}^+ \to \mathrm{K}^+\mathrm{X}$ signal fixed from simulation.
- The J/ψ ($\psi(2\mathrm{S})$) resonant background leakage to nearby q^2 bins is described with a DCB function with the normalization as a free parameter of the fit and the shape parameters fixed by fitting simulated $\mathrm{B}^+ \to \mathrm{J}/\psi(\mu^+\mu^-)\mathrm{K}^+$ ($\mathrm{B}^+ \to \psi(2\mathrm{S})(\mu^+\mu^-)\mathrm{K}^+$) events in the specific q^2 bin. This contribution is included only in the simultaneous fit in the following q^2 bins: 6.0–7.0 and 7.0–8.0 GeV^2 for the $\mathrm{B}^+ \to \mathrm{J}/\psi(\mu^+\mu^-)\mathrm{K}^+$ background, and 11.0–11.8, 11.8–12.5, and 14.82–16.0 GeV^2 for the $\mathrm{B}^+ \to \psi(2\mathrm{S})(\mu^+\mu^-)\mathrm{K}^+$ background.

For the $\mathrm{B}^+ \to \mathrm{J}/\psi(\mu^+\mu^-)\mathrm{K}^+$ CRs, the fit is kept as close as possible to the single fit in the low-q^2 region in terms of template functions and parameter treatment. Nevertheless, because of the much smaller radiative tail due to the tight $2.9 < m_{\mu^+\mu^-} < 3.2\,\mathrm{GeV}$ requirement in the J/ψ CR and the different background sources, some of the templates are different from the ones used for nonresonant signal. The signal is described by a sum of three Gaussian functions with all shape parameters constrained within the uncertainties from a fit to simulated data. The $\mathrm{B}^+ \to \mathrm{J}/\psi(\mu^+\mu^-)\mathrm{K}^*(892)^+$ background is described with the sum of a DCB function and an exponential function, with all the shape parameters fixed from simulation, as in the 11.0–19.24 GeV^2 q^2 range of the simultaneous fit.

The $\mathrm{B}^+ \to \psi(2\mathrm{S})(\mu^+\mu^-)\mathrm{K}^+$ CR is not used directly in the analysis, but is utilized for several cross checks (such as the $R_{\psi(2\mathrm{S})}$ measurement). For validation purposes, the functions used for the fit in the $\mathrm{B}^+ \to \psi(2\mathrm{S})(\mu^+\mu^-)\mathrm{K}^+$ CR are exactly the same as in the low-q^2 region, except for the $\mathrm{B}^+ \to \mathrm{J}/\psi(\mu^+\mu^-)\mathrm{K}^*(892)^+$ background, which is described with the sum of a DCB function and an exponential function with all the shape parameters fixed from simulation, as in the 11–19.24 GeV^2 q^2 range of the simultaneous fit.

Table 4. Fit functions used for signal and background sources in each q^2 bin in the muon channel. The—symbol indicates this background is not included in this region.

Process	$B^+ \to K^+\mu^+\mu^-$	$B^+ \to J/\psi(\mu^+\mu^-)K^+$	$B^+ \to \psi(2S)(\mu^+\mu^-)K^+$
Signal	DCB + Gaussian	Sum of 3 Gaussians	DCB + Gaussian
Comb. & other b bkg.	Exponential[a]	Exponential	Exponential
$B^+ \to K^*(892)^{0/+}X$	DCB (+ expon.)	DCB + exponential	DCB + exponential
$B^+ \to \pi^+X$	DCB	DCB	DCB
$B^+ \to J/\psi(\mu^+\mu^-)K^+$	DCB (nearby q^2)	—	—
$B^+ \to \psi(2S)(\mu^+\mu^-)K^+$	DCB (nearby q^2)	—	—

[a] In the last q^2 bin the exponential function is multiplied by $m_{K^+\mu^+\mu^-} - m_{\mu^+\mu^-} - m_{K}^{+}$ to account for the phase space suppression.

Table 5. Signal yields in the muon channel in the low-q^2 bin and resonant CRs.

Channel	q^2 range [GeV^2]	Yield
$B^+ \to K^+\mu^+\mu^-$	1.1–6.0	1267 ± 55
$B^+ \to J/\psi(\mu^+\mu^-)K^+$	8.41–10.24	$728\,000 \pm 1000$
$B^+ \to \psi(2S)(\mu^+\mu^-)K^+$	12.60–14.44	$68\,300 \pm 500$

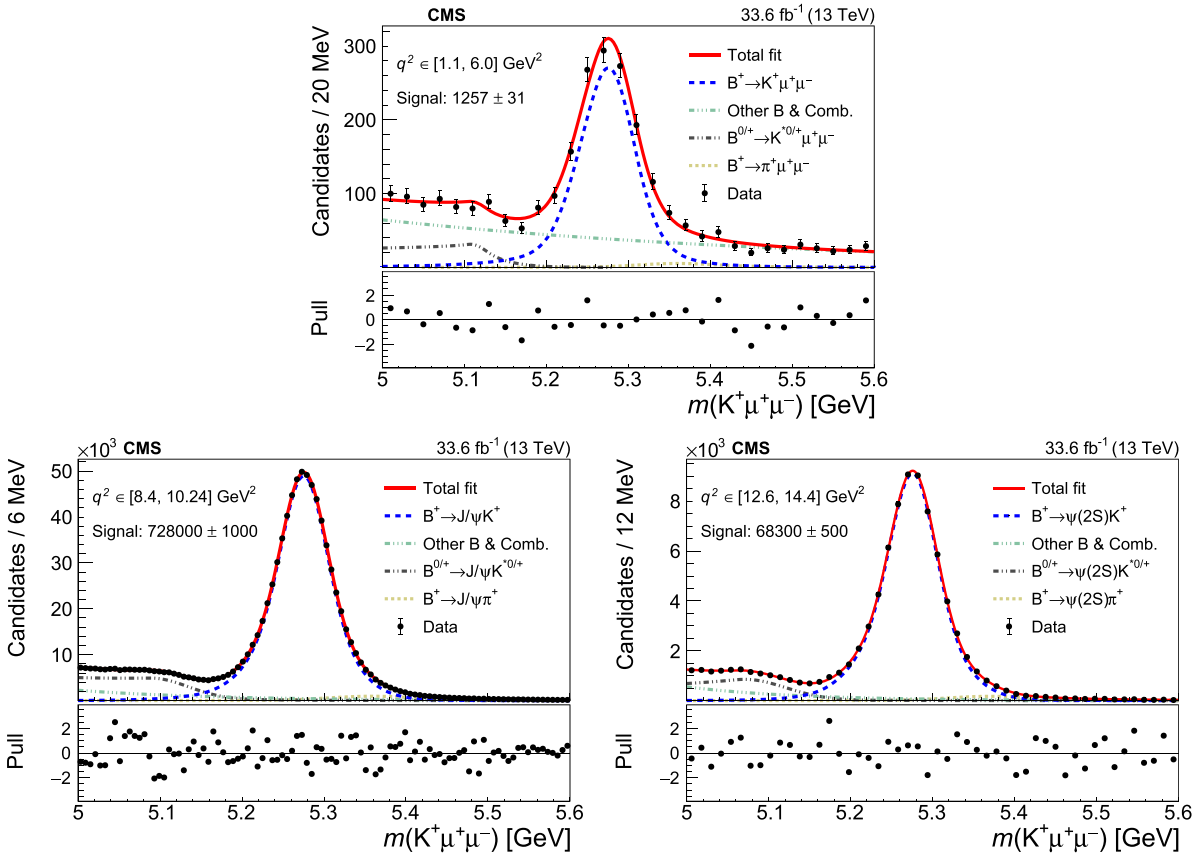

Figure 3. Results of an unbinned likelihood fit to the $K^+\mu^+\mu^-$ invariant mass distributions in the low-q^2 bin (upper), and in the $B^+ \to J/\psi(\mu^+\mu^-)K^+$ (lower left) and $B^+ \to \psi(2S)(\mu^+\mu^-)K^+$ (lower right) CRs. The error bars show the statistical uncertainty in data. The lower panels show the distribution of the pull, which is defined as the Poisson probability to observe the number of event counts in data, given the fit function, expressed in terms of the Gaussian significance.

The functions used in the fit are summarized in table 4. The results of the unbinned maximum likelihood fit, with the systematic uncertainties represented by the nuisance parameters in the likelihood with Gaussian priors, are shown in table 5 and figure 3 for the low-q^2 bin and resonant CRs and in table 10 and figures A3–A4 for the simultaneous fit.

Table 6. Fit functions used to describe signal and various background components for the electron channel. The — symbol indicates this background is not included in this region.

Process	$B^+ \to K^+e^+e^-$	$B^+ \to J/\psi(e^+e^-)K^+$	$B^+ \to \psi(2S)(e^+e^-)K^+$
Signal	DCB function	CB + Gaussian	CB + Gaussian
Comb. background	Exponential	Exponential	Exponential
$B^+ \to K^*(892)^{0/+}X$	—	KDE template	KDE template
$B^+ \to \pi^+X$	—	CB function	—
$B^+ \to J/\psi(e^+e^-)K^+$	KDE template	—	—
Other b decays	—	KDE template	KDE template

Table 7. Signal yields in the electron channel in the low-q^2 bin and resonant CRs.

Channel	q^2 range [GeV^2]	PF-PF yield	PF-LP yield
$B^+ \to K^+e^+e^-$	1.1–6.0	17.9 ± 7.2	3.0 ± 5.9
$B^+ \to J/\psi(e^+e^-)K^+$	8.41–10.24	4857 ± 84	2098 ± 58
$B^+ \to \psi(2S)(e^+e^-)K^+$	12.60–14.44	320 ± 20	94 ± 11

6.3. Electron channel signal extraction

To extract the number of signal events, unbinned maximum likelihood fits to the B^+ candidate invariant mass distribution are performed in three q^2 regions. The q^2 regions considered are: low-q^2 aiming at the signal $B^+ \to K^+e^+e^-$ decay, and two CRs aiming at $B^+ \to J/\psi(e^+e^-)K^+$ and $B^+ \to \psi(2S)(e^+e^-)K^+$ decays. The high-q^2 bin, above the $\psi(2S)$ resonance, has been studied, but the backgrounds in this bin are too large to extract the $B^+ \to K^+e^+e^-$ signal reliably; consequently, it is not included in the analysis. Fits are done independently in the PF-PF and PF-LP categories. Signal shapes are described by either a DCB function or the sum of a one-sided crystal ball (CB) function [72] and a Gaussian function. The same background sources as in the muon channel also contribute here, albeit with different relative importance. The partially reconstructed background is similar to that in the muon channel. The combinatorial background is more prominent with respect to the muon channel, because of the higher fraction of hadrons misreconstructed as electrons. Finally, the other b hadron decay background is represented by a separate template. In the electron channel, we use simulated distributions directly to construct various background templates. This is achieved using the kernel density estimator (KDE) method [74] applied to simulated events. The only exception is the combinatorial background, for which a simple exponential with the slope and normalization floating in the fit is used. The Cabibbo-suppressed decay background is negligible for the low-q^2 and $\psi(2S)$ bins, and therefore is accounted for only in the $B^+ \to J/\psi(e^+e^-)K^+$ CR. The relative normalization of this background to the signal is fixed from simulation. The shapes of various backgrounds are fixed from simulation and the normalizations are free parameters of the fit, unless specified otherwise. The functions used in the fit are presented in table 6. Figure 4 shows the $K^+e^+e^-$ invariant mass distribution for the electron channels in the three q^2 regions for the PF-PF and PF-LP categories. The signal yields in these regions are listed in table 7.

7. Systematic uncertainties

Statistical uncertainties in the signal yields are propagated into the measurement of $R(K)$. The final statistical uncertainty in $R(K)$ is dominated by the yield in the low-q^2 bin in the electron channel, which is of order of 40% (as can be seen in figure 4).

Systematic uncertainties in this analysis fall into two categories: those due to the finite size of the signal MC samples used for the $\mathcal{A}\epsilon$ estimates, which are statistical in nature, and those that reflect certain assumptions made in the analysis. Systematic uncertainties are calculated independently for the muon and electron channel parts of $R(K)$, because they largely cancel in the single ratios, $B^+ \to K^+\ell^+\ell^-/B^+ \to J/\psi(\ell^+\ell^-)K^+$, in each of the two channels. Consequently, only the uncertainties that do not cancel or cancel partially are discussed in this section. The uncertainties in the muon and electron channels are treated as uncorrelated, which is supported by the fact that the two channels have different sources of systematic uncertainties due to differences in the trigger, kinematics (because of the tag-side vs. probe-side selection), and lepton reconstruction. To evaluate the impact of a systematic source, the $R(K)$ ratio is remeasured after changing the central value for the source under study by $\pm 1\sigma$. The difference between the modified and nominal values of the single ratio is used as the systematic uncertainty.

7.1. Systematic uncertainties in the muon channel single ratio

The dominant systematic uncertainties in the single ratio $B^+ \to K^+\mu^+\mu^-/B^+ \to J/\psi(\mu^+\mu^-)K^+$, in order of importance, are as follows:

- Parameterization of the background function of the $B^+ \to K^+\mu^+\mu^-$ fit: this uncertainty is estimated by using a falling tail of a Gaussian function instead of an exponential function to describe the dominant combinatorial plus other B meson decays background. The effect is 1.8%.

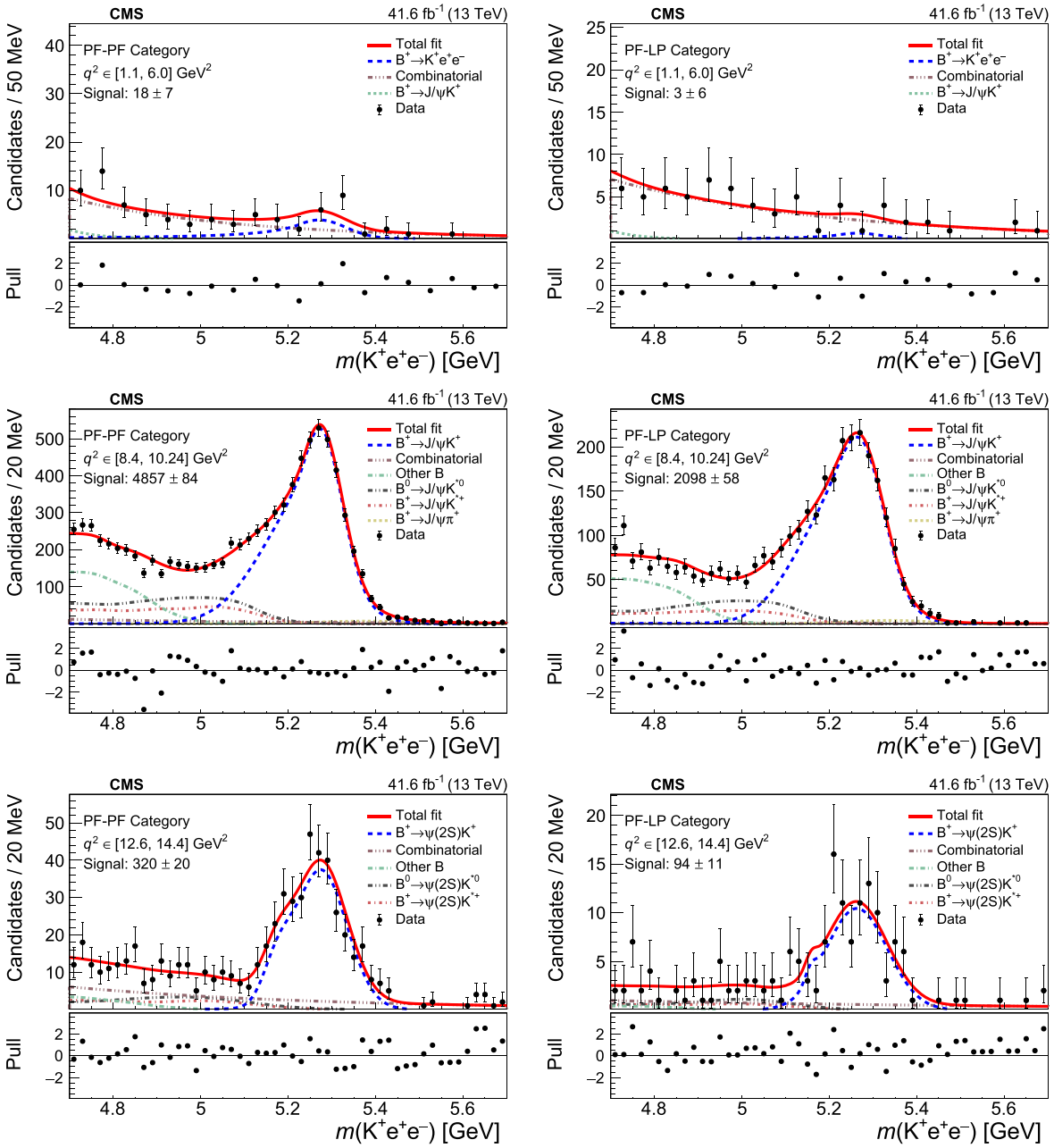

Figure 4. The $K^+e^+e^-$ invariant mass spectrum with the results of the fit shown with the red line in the low-q^2 region (upper row), $B^+ \to J/\psi(e^+e^-)K^+$ CR (middle row), and $B^+ \to \psi(2S)(e^+e^-)K^+$ CR (lower row) for the PF-PF (left column) and PF-LP (right column) categories. The shoulder below the nominal B^+ meson mass for the $\psi(2S)$ CR is due to the narrow q^2 range in this bin compared to the size of the radiative tail. Notations are as in figure 3.

- Operating below the trigger plateau: the uncertainty in the trigger turn-on effects was estimated by repeating the measurement after tightening the offline requirements. The corresponding uncertainty is 1.3%.
- Uncertainty in the FONLL SFs: simulated events are reweighted in p_T and rapidity of the B candidate according to the FONLL predictions. The corresponding uncertainty is 0.9%.
- Parameterization of the background function in the $B^+ \to J/\psi(\mu^+\mu^-)K^+$ CR fit: the uncertainty is estimated the same way as in the SR. The effect is 0.6%.
- Description of the J/ψ meson radiative tail: events in the $B^+ \to J/\psi(\mu^+\mu^-)K^+$ channel are selected using a fixed q^2 window. A mismodeling of the tail can lead to an incorrect calculation of efficiency. This effect is estimated by repeating the measurement in a larger q^2 window, by relaxing the lower boundary from 2.9 to 2.8 GeV. The effect is 0.5%.
- Pileup: the pileup profile is reweighted using a ±4.6% variation in the total inelastic pp cross section [75]. The corresponding uncertainty is 0.4%.
- Parameterization of the signal shape in the low-q^2 $B^+ \to K^+\mu^+\mu^-$ fit: the uncertainty due to the signal description is

Table 8. Major sources of uncertainty in the $B^+ \to K^+\mu^+\mu^-$/ $B^+ \to J/\psi(\mu^+\mu^-)K^+$ ratio measurement.

Source	Impact on the $R(K)$ ratio (%)
Background description, low-q^2 bin	1.8
Trigger turn-on	1.3
Reweighting in p_T and rapidity	0.9
Background description, J/ψ CR	0.6
J/ψ meson radiative tail description	0.5
Pileup	0.4
Signal shape description	0.3
Trigger efficiency	0.2
J/ψ resonance shape description	0.1
Nonresonant contribution to the J/ψ CR	0.1
Total systematic uncertainty	2.6
Statistical uncertainty in MC samples	1.7
Statistical uncertainty in data	7.5
Total uncertainty	8.1

estimated by adding an extra Gaussian function to the signal template and repeating the fit. The corresponding systematic uncertainty is 0.3%.

- Uncertainty in the trigger SFs: the combined statistical and systematic uncertainty from the SF measurement is obtained using the tag-and-probe method. The effect is 0.2%.
- Parameterization of the signal shape in the $B^+ \to J/\psi(\mu^+\mu^-)K^+$ fit: this uncertainty is evaluated in the same way as in the low-q^2 bin. The corresponding uncertainty is 0.1%.
- The nonresonant $B^+ \to K^+\mu^+\mu^-$ contribution in the $B^+ \to J/\psi(\mu^+\mu^-)K^+$ CR: the predicted $B^+ \to K^+\mu^+\mu^-$ contribution in the J/ψ q^2 range using PYTHIA is subtracted from the signal yield. The effect is 0.1%.

Other uncertainty sources were also studied (e.g. several SFs related to the BDT), but found to have a negligible effect (<0.01%) and are therefore omitted. The systematic sources are treated as uncorrelated, and the overall uncertainty in the low-q^2 bin is found to be 2.6%. The statistical uncertainty in the same bin is 7.5% and the uncertainty from the limited size of the simulation sample used for the $\mathcal{A}\epsilon$ calculations is 1.7%. The uncertainties in the $B^+ \to K^+\mu^+\mu^-/B^+ \to J/\psi(\mu^+\mu^-)K^+$ ratio measurement are summarized in table 8. For the differential branching fraction measurement the same systematic sources are evaluated in each q^2 bin and the resulting uncertainties are shown in figure A2. In most q^2 bins, the data statistical uncertainty is dominant.

7.2. Systematic uncertainties in the electron channel single ratio

Since the yield of $B^+ \to K^+e^+e^-$ events in the low-q^2 bin is small, the overall uncertainty is dominated by the statistical uncertainty. The sources of systematic uncertainties in the electron channel are generally different from those in the muon channel, due to different kinematics and reconstruction performance.

The dominant uncertainties in the single ratio $B^+ \to K^+e^+e^-/B^+ \to J/\psi(e^+e^-)K^+$, in order of importance, are as follows:

- Parameterization of signal and background shapes: both the signal and background shapes in the fits of the low-q^2 SR and J/ψ CR are modified and the difference is taken as an uncertainty. The modification is done by replacing the KDE-based templates with analytical functions similar to the ones used in the muon channel. The signal description in the low-q^2 bin was modified by adding an extra Gaussian function, and the exponential describing the combinatorial background was replaced by a second-order Chebyshev polynomial. The combined uncertainty in the fit parameterization because of the signal and background variations is about 5% each in the PF-PF and PF-LP categories.
- Constraint on the $B^+ \to J/\psi(e^+e^-)K^+$ contribution: the normalization of the J/ψ meson leakage background in the $B^+ \to K^+e^+e^-$ channel in the low-q^2 region is constrained to the expected yield from the fit in the $B^+ \to J/\psi(e^+e^-)K^+$ CR. The uncertainty is dominated by the statistical uncertainty in the yield of this background and is estimated using pseudo-experiments, while the contribution from the radiative tail mismodeling is negligible. The uncertainty amounts to 4 (9)% in the PF-PF (PF-LP) category.
- The BDT efficiency stability: the BDT WP is chosen to maximize the expected significance of the $B^+ \to K^+e^+e^-$ signal in the low-q^2 region. A variation of the WP corresponding to a variation of $\pm 10\%$ in the expected significance is chosen to evaluate the stability. The corresponding systematic uncertainty is 2 (5)% for the PF-PF (PF-LP) category.
- The BDT cross-validation: to allow for the entire data set to be used both in the BDT training and testing, an eight-fold cross validation is used, resulting in eight different BDTs. The spread in the efficiency of these BDTs is used as the uncertainty, amounting to 2 (3)% in the PF-PF (PF-LP) category.
- Triggers in the B parking data set: in the electron channel all the B parking triggers are used for the measurement. The small kinematical correlation between the tag and probe sides could have an impact on the $R(K)$ value. Due to a complicated mixture of L1 and HLT triggers, some of which are prescaled as a function of the instantaneous luminosity, the composition in terms of trigger paths is different in simulated samples than in data. To account for this, the trigger efficiency ratio between the low-q^2 SR and J/ψ CR is estimated for several individual trigger paths and the variation of this ratio is taken as a systematic uncertainty amounting to 1 (4)% for the PF-PF (PF-LP) category.
- The BDT SF: this SF accounts for the differences in the BDT WP efficiency between data and simulation. The efficiency of the nominal WP with respect to a loose selection, which is nearly fully efficient for signal, is computed in the J/ψ CR, and transferred to the low-q^2 bin using simulation. The

Table 9. Major sources of uncertainty in the $B^+ \to K^+e^+e^-/B^+ \to J/\psi(e^+e^-)K^+$ ratio measurement in the PF-PF and PF-LP categories. The last row shows the statistical uncertainty, which is the same as the total uncertainty within the quoted precision.

	Impact on the $R(K)$ ratio (%)	
Source	PF-PF	PF-LP
Signal and background description	5	5
J/ψ event leakage to the low-q^2 bin	4	9
BDT efficiency stability	2	5
BDT cross validation	2	3
Trigger efficiency	1	4
BDT data/simulation difference	1	2
J/ψ meson radiative tail description	1	1
Total systematic uncertainty	7	13
Statistical and total uncertainty	40	200

uncertainty from this source is 1 (2)% in the PF-PF (PF-LP) category.

- Description of the J/ψ meson radiative tail: this uncertainty is estimated in the same way as in the muon channel, except that the enlargement of the q^2 window is bigger in the case of electrons to account for the larger radiative tail. The effect is 1% for both PF-PF and PF-LP categories.

Other sources of uncertainty have an impact of less than 1% on the $B^+ \to K^+e^+e^-/B^+ \to J/\psi(e^+e^-)K^+$ ratio. The reason the uncertainties in the BDT performance are much larger in the electron channel than in the muon one is the much tighter WP used, which results in effectively smaller training samples and higher sensitivity to data-to-simulation differences in the tails of the distributions of the various input variables. All sources of systematic uncertainties are treated as uncorrelated, which results in an overall systematic uncertainty in the $B^+ \to K^+e^+e^-/B^+ \to J/\psi(e^+e^-)K^+$ single ratio of 7 and 13% for the PF-PF and PF-LP categories, respectively. The systematic uncertainties are small compared to the statistical ones which are 40 (200)% for the PF-PF (PF-LP) channel. Table 9 summarizes the uncertainties in the electron channel.

8. Results

In this section, we report the following results:

- measurement of the differential branching fraction of the $B^+ \to K^+\mu^+\mu^-$ decay in the full q^2 range, excluding the J/ψ and $\psi(2S)$ resonances;
- measurement of the integrated branching fractions of the $B^+ \to K^+\mu^+\mu^-$ decay in the low-q^2 region and in the full q^2 range; and
- measurement of $R(K)$ in the low-q^2 region.

To validate the analysis procedure we performed several cross-checks, the two most important ones being the measurement of the $R_{\psi(2S)}$ and $R_{J/\psi}$ ratios. The former is defined by equation (3), i.e. exchanging the $B^+ \to K^+\ell^+\ell^-$ decay by the $B^+ \to \psi(2S)(\ell^+\ell^-)K^+$ one. The latter is the ratio of the $B^+ \to J/\psi(\mu^+\mu^-)K^+$ and $B^+ \to J/\psi(e^+e^-)K^+$ branching fractions. Both these ratios are expected and measured [4] to be flavor-universal (i.e. equal to unity), with high precision. An important added value of the $R_{J/\psi}$ cross-check is that various efficiencies and corrections that cancel out in the $R(K)$ double ratio, only partially cancel or do not cancel in the $R_{J/\psi}$ single ratio. Therefore, this cross check also validates the systematic uncertainties that cancel in the $R(K)$ ratio.

The results of our measurement in the combination of the PF-PF and PF-LP categories are: $R_{\psi(2S)} = 0.966^{+0.071}_{-0.066}$ and $R_{J/\psi} = 1.006^{+0.020}_{-0.019}$, where the uncertainties shown are statistical only. Both the $R_{\psi(2S)}$ and $R_{J/\psi}$ measurements are consistent with unity within one standard deviation, with a precision of a few percent. The systematic uncertainty due to the lack of cancellation of various efficiencies and from sources discussed in section 7 for both ratios is estimated to be around 7%. Consistent results are obtained in the PF-PF and PF-LP categories separately, albeit with larger statistical uncertainties.

8.1. Measurement of the differential $\mathcal{B}(B^+ \to K^+\mu^+\mu^-)$

To reduce the systematic uncertainty, the differential branching fraction in each q^2 bin is normalized to $\mathcal{B}(B^+ \to J/\psi(\mu^+\mu^-)K^+)$,

$$\begin{aligned}\mathcal{B}\left(B^+ \to K^+\mu^+\mu^-\right)\left[q^2_{\min}, q^2_{\max}\right] &= \frac{N_{B^+\to K^+\mu^+\mu^-}\left[q^2_{\min}, q^2_{\max}\right]}{N_{B^+\to J/\psi(\mu^+\mu^-)K^+}\left[8.41, 10.24\right]\text{GeV}^2} \\ &\times \frac{\left(\mathcal{A}\epsilon\epsilon_{\text{trig}}\right)_{B^+\to J/\psi(\mu^+\mu^-)K^+}\left[8.41, 10.24\right]\text{GeV}^2}{\left(\mathcal{A}\epsilon\epsilon_{\text{trig}}\right)_{B^+\to K^+\mu^+\mu^-}\left[q^2_{\min}, q^2_{\max}\right]} \\ &\times \mathcal{B}\left(B^+ \to J/\psi K^+\right)\mathcal{B}\left(J/\psi \to \mu^+\mu^-\right), \end{aligned} \quad (4)$$

where $N_{B^+\to K^+\mu^+\mu^-}$ and $N_{B^+\to J/\psi(\mu^+\mu^-)K^+}$ are the measured yields from the fit in the q^2 region indicated in the brackets and $\mathcal{B}(B^+ \to J/\psi(\mu^+\mu^-)K^+)$ is the world-average value of the $B^+ \to J/\psi(\mu^+\mu^-)K^+$ branching fraction [4]. The measured differential branching fraction of the $B^+ \to K^+\mu^+\mu^-$ decay is summarized in table 10. The correlation matrix between the extracted values of the differential branching fraction in different q^2 bins is shown in figure A5.

Since there are various and somewhat different theoretical predictions for the SM value of $\mathrm{d}(\mathcal{B}(B^+ \to K^+\mu^+\mu^-)/q^2$, we compare our measurement with the predictions from the HEPFIT [27, 76–78] v1.0, SUPERISO [79, 80] v4.1, FLAVIO [81] v2.5.5, and EOS [82, 83] v1.0.8 packages. These models rely on different approaches in evaluating the effects of nonlocal form-factor contributions, which is reflected in a sizable difference between the uncertainties in their predictions. None of the calculations can reliably describe the regions between the J/ψ and $\psi(2S)$ resonances; hence the predictions are not shown in this q^2 range. In addition, the HEPFIT package only gives predictions for $q^2 < 8\,\text{GeV}^2$. The comparison of our measurement with the prediction of these models is shown in

Table 10. The $B^+ \to K^+\mu^+\mu^-$ branching fraction, $d(\mathcal{B}(B^+ \to K^+\mu^+\mu^-)/q^2$ integrated over the specified q^2 range, for the individual q^2 bins.. The uncertainties in the yields are statistical uncertainties from the fit, while the branching fraction uncertainties include both the statistical and systematic components.

q^2 range (GeV^2)	Signal yield	Branching fraction (10^{-8})
0.1–0.98	260 ± 20	2.91 ± 0.24
1.1–2.0	197 ± 19	1.93 ± 0.20
2.0–3.0	306 ± 23	3.06 ± 0.25
3.0–4.0	260 ± 21	2.54 ± 0.23
4.0–5.0	251 ± 23	2.47 ± 0.24
5.0–6.0	264 ± 27	2.53 ± 0.27
6.0–7.0	267 ± 21	2.50 ± 0.23
7.0–8.0	256 ± 23	2.34 ± 0.25
11.0–11.8	207 ± 19	1.62 ± 0.18
11.8–12.5	172 ± 16	1.26 ± 0.14
14.82–16.0	272 ± 20	1.83 ± 0.17
16.0–17.0	246 ± 17	1.57 ± 0.15
17.0–18.0	317 ± 19	2.11 ± 0.16
18.0–19.24	242 ± 19	1.74 ± 0.15
19.24–22.9	158 ± 19	2.02 ± 0.30

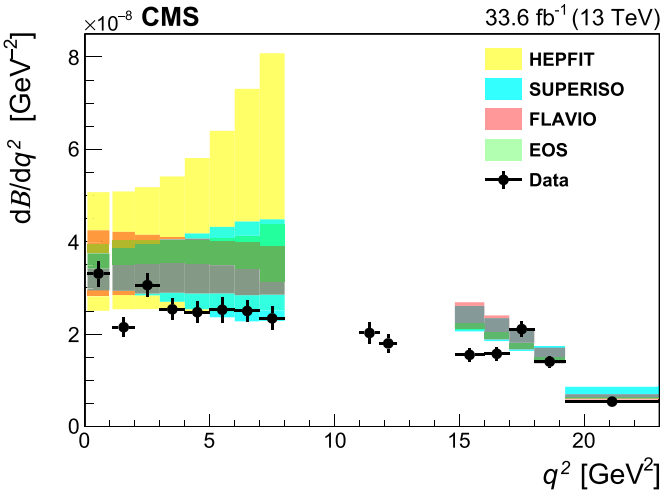

Figure 5. Comparison of the measured differential $B^+ \to K^+\mu^+\mu^-$ branching fraction with the theoretical predictions obtained using HEPFIT, SUPERISO, FLAVIO, and EOS packages. The HEPFIT predictions are available only for $q^2 < 8\,\mathrm{GeV}^2$.

figure 5. The measured differential branching fraction of the $B^+ \to K^+\mu^+\mu^-$ decay is generally lower than the theoretical predictions for $q^2 < 17\,\mathrm{GeV}^2$, which is consistent with the results reported by LHCb [23, 24].

8.2. Measurement of the integrated $\mathcal{B}(B^+ \to K^+\mu^+\mu^-)$

The low-q^2 region is especially interesting because it is not affected by higher-mass resonances and their interference effects. Consequently, the branching fraction of the $B^+ \to K^+\mu^+\mu^-$ decay in this q^2 region can be measured with relatively little theoretical dependence, using equation (4) over the $[1.1, 6.0]\,\mathrm{GeV}^2$ q^2 range. In this range, the acceptance times efficiency is essentially independent of the q^2 value, as shown in figure A1. Therefore, any dependence on theory can only arise from residual differences in the kinematic distributions of the final-state particles between theory and data. Since the acceptance times efficiency is evaluated using events generated with the EVTGEN $B^+ \to K^+\mu^+\mu^-$ model (discussed in section 4.2), which has been tuned using e^+e^- experimental data, as well as lattice calculations, any such residual differences are expected to be minimal. The resulting measurement is

$$\begin{aligned}\mathcal{B}\left(B^+ \to K^+\mu^+\mu^-\right)[1.1, 6.0]\,\mathrm{GeV}^2 \\ = (12.42 \pm 0.54\,(\mathrm{stat}) \pm 0.11\,(\mathrm{MC\ stat}) \pm 0.40\,(\mathrm{syst})) \\ \times 10^{-8} = (12.42 \pm 0.68) \times 10^{-8}. \end{aligned} \quad (5)$$

This result is consistent with the present world-average value of $(12.6 \pm 1.2) \times 10^{-8}$ [4] in a very similar range, $1.0 < q^2 < 6.0\,\mathrm{GeV}^2$, and has a 40% smaller uncertainty. It is also consistent with and has a similar uncertainty as the LHCb measurement [24] in the $1.1 < q^2 < 6.0\,\mathrm{GeV}^2$ range, $(11.86 \pm 0.68) \times 10^{-8}$, which presently dominates the world-average value. (The larger uncertainty in the world-average value is due to a SF of 1.9 introduced to address the tension between the individual results.) The comparison between our measurement and the theoretical predictions described above is shown in table 11. All of the theoretical estimates are higher than our measurement in the low-q^2 region.

Table 11. Comparison of the $\mathcal{B}(B^+ \to K^+\mu^+\mu^-)$ branching fraction measurement in the low-q^2 range and the theoretical predictions based on the EOS, FLAVIO, SUPERISO, and HEPFIT packages.

Source	$\mathcal{B}(B^+ \to K^+\mu^+\mu^-)[1.1, 6.0]\,\mathrm{GeV}^2$ (10^{-8})
Measurement	12.42 ± 0.68
EOS	18.9 ± 1.3
FLAVIO	17.1 ± 2.7
SUPERISO	16.5 ± 3.4
HEPFIT	19.8 ± 7.3

In order to determine the integrated $\mathcal{B}(B^+ \to K^+\mu^+\mu^-)$, the result of equation (5) must be divided by the fraction of events in the low-q^2 bin. This fraction cannot be taken directly from data because of the interference effects and resonant contributions. Two theoretical models are used to obtain the differential branching fraction distribution in the full q^2 range, based on the FLAVIO and SUPERISO packages. The resulting $\mathcal{B}(B^+ \to K^+\mu^+\mu^-)$ integrated branching fractions are $43.5 \pm 1.9(\mathrm{stat}) \pm 0.4\,(\mathrm{MC\ stat}) \pm 1.4(\mathrm{syst}) = 43.5 \pm 2.4$ (FLAVIO) and $43.9 \pm 1.9(\mathrm{stat}) \pm 0.4\,(\mathrm{MC\ stat}) \pm 1.4(\mathrm{syst}) = 43.9 \pm 2.4$ (SUPERISO), where the theoretical model uncertainty is not included. Both results are in good agreement with the world-average value of $(45.3 \pm 3.5) \times 10^{-8}$ [4], as well as with the LHCb measurement of $(43.7 \pm 2.7) \times 10^{-8}$ that explicitly subtracts various resonant contributions [84]. For the calculation of the integrated branching fraction $\mathcal{B}(B^+ \to K^+\mu^+\mu^-)$, only FLAVIO and SUPERISO are used

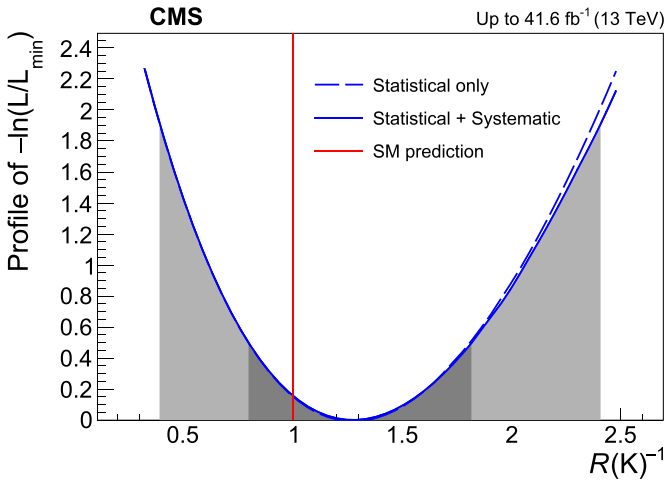

Figure 6. Log likelihood function from the fit profiled as a function of $R(\mathrm{K})^{-1}$. The dark and light grey area indicates the ± 1 and $\pm 2\,\sigma$ bands respectively.

because EOS and HEPFIT do not provide predictions for the entire q^2 range.

8.3. Measurement of $R(K)$

For the $R(\mathrm{K})$ measurement, both the $\mathrm{B}^+ \to \mathrm{K}^+\mu^+\mu^-$ and $\mathrm{B}^+ \to \mathrm{K}^+\mathrm{e}^+\mathrm{e}^-$ channels are used in the low-q^2 region, along with the $\mathrm{B}^+ \to \mathrm{J}/\psi(\mu^+\mu^-)\mathrm{K}^+$ and $\mathrm{B}^+ \to \mathrm{J}/\psi(\mathrm{e}^+\mathrm{e}^-)\mathrm{K}^+$ CRs, separately in the PF-PF and PF-LP electron channel categories and in their combination,. The details are given in appendix A.2. The systematic uncertainties are incorporated into the likelihood function assuming Gaussian distributions. The correlation of a few minor uncertainties between the two channels were found to have a negligible effect on the results. A profile likelihood is used to obtain the confidence interval of the parameter of interest, $R(\mathrm{K})^{-1}$.

The values of $R(\mathrm{K})^{-1}$ extracted in the PF-PF and PF-LP categories are $1.40^{+0.63}_{-0.56}$ and $0.50^{+1.06}_{-0.88}$, respectively, where the uncertainties are statistical only. These values are consistent with each other and with unity. As expected from the corresponding signal yields, the PF-PF result is much more precise. The maximum likelihood fit for the combination of the PF-PF and PF-LP categories gives $R(\mathrm{K})^{-1} = 1.28^{+0.53}_{-0.47}$, where the uncertainties are statistical only. The profile log likelihood of the combined fit, $\ln(L/L_{\mathrm{min}})$, as a function of $R(\mathrm{K})^{-1}$ is shown in figure 6. The measurement of $R(\mathrm{K})$ and its 68% confidence interval can be obtained from those for $R(\mathrm{K})^{-1}$,

$$R(\mathrm{K}) = 0.78^{+0.46}_{-0.23}\,(\mathrm{stat})^{+0.09}_{-0.05}\,(\mathrm{syst}) = 0.78^{+0.47}_{-0.23}, \qquad (6)$$

which is within one standard deviation from the SM prediction of approximately unity. The summary of the available $R(K)$ measurements is shown in figure A6.

9. Summary

We have reported the first test of LFU with the CMS experiment at the LHC in $\mathrm{B}^\pm \to \mathrm{K}^\pm\mu^+\mu^-$ and $\mathrm{B}^\pm \to \mathrm{K}^\pm\mathrm{e}^+\mathrm{e}^-$ decays, as well as a measurement of differential and integrated branching fractions of the nonresonant $\mathrm{B}^\pm \to \mathrm{K}^\pm\mu^+\mu^-$ decay. The analysis has been made possible by a dedicated data set of proton-proton collisions at $\sqrt{s} = 13\,\mathrm{TeV}$ recorded in 2018, using a special high-rate data stream designed for collecting about 10 billion unbiased b hadron decays. The ratio of the branching fractions $\mathcal{B}(\mathrm{B}^\pm \to \mathrm{K}^\pm\mu^+\mu^-)$ to $\mathcal{B}(\mathrm{B}^\pm \to \mathrm{K}^\pm\mathrm{e}^+\mathrm{e}^-)$ has been is determined from the measured double ratio $R(\mathrm{K})$ of these decays to the respective branching fractions of the $\mathrm{B}^\pm \to \mathrm{J}/\psi\mathrm{K}^\pm$ $(\mathrm{J}/\psi \to \mu^+\mu^-)$ and $(\mathrm{J}/\psi \to \mathrm{e}^+\mathrm{e}^-)$ decays, which allow for significant cancellation of systematic uncertainties. The ratio $R(\mathrm{K})$ has been measured in the range $1.1 < q^2 < 6.0\,\mathrm{GeV}^2$, where q is the invariant mass of the lepton pair, and was found to be $R(\mathrm{K}) = 0.78^{+0.47}_{-0.23}$, in agreement with the SM expectation of $\approx$1. This measurement is limited by the statistical precision of the electron channel. The integrated branching fraction in the same q^2 range, $\mathcal{B}(\mathrm{B}^\pm \to \mathrm{K}^\pm\mu^+\mu^-) = (12.42 \pm 0.68) \times 10^{-8}$, is consistent with and has a comparable precision to the present world average. This work has demonstrated the flexibility of the CMS trigger and data acquisition system and has paved the way to many other studies of a large unbiased sample of b hadron decays collected by CMS in 2018.

Data availability statement

Release and preservation of data used by the CMS Collaboration as the basis for publications is guided by the CMS policy as stated in CMS data preservation, reuse and open access policy https://cms-docdb.cern.ch/cgi-bin/PublicDocDB/RetrieveFile?docid=6032&filename=CMSDataPolicyV1.2.pdf&version=2.

Acknowledgments

We congratulate our colleagues in the CERN accelerator departments for the excellent performance of the LHC and thank the technical and administrative staffs at CERN and at other CMS institutes for their contributions to the success of the CMS effort. In addition, we gratefully acknowledge the computing centers and personnel of the Worldwide LHC Computing Grid and other centers for delivering so effectively the computing infrastructure essential to our analyses. Finally, we acknowledge the enduring support for the construction and operation of the LHC, the CMS detector, and the supporting computing infrastructure provided by the following funding agencies: SC (Armenia), BMBWF and FWF (Austria); FNRS and FWO (Belgium); CNPq, CAPES, FAPERJ, FAPERGS, and FAPESP (Brazil); MES and BNSF (Bulgaria); CERN; CAS, MoST, and NSFC (China); MINCIENCIAS (Colombia); MSES and CSF (Croatia); RIF (Cyprus); SENESCYT (Ecuador); MoER, ERC PUT and ERDF (Estonia); Academy of Finland, MEC, and HIP (Finland); CEA and CNRS/IN2P3 (France); SRNSF (Georgia); BMBF, DFG, and HGF (Germany); GSRI (Greece); NKFIH (Hungary); DAE and DST (India); IPM (Iran); SFI (Ireland); INFN (Italy); MSIP and NRF (Republic

of Korea); MES (Latvia); LAS (Lithuania); MOE and UM (Malaysia); BUAP, CINVESTAV, CONACYT, LNS, SEP, and UASLP-FAI (Mexico); MOS (Montenegro); MBIE (New Zealand); PAEC (Pakistan); MES and NSC (Poland); FCT (Portugal); MESTD (Serbia); MCIN/AEI and PCTI (Spain); MOSTR (Sri Lanka); Swiss Funding Agencies (Switzerland); MST (Taipei); MHESI and NSTDA (Thailand); TUBITAK and TENMAK (Turkey); NASU (Ukraine); STFC (United Kingdom); DOE and NSF (USA).

Individuals have received support from the Marie-Curie program and the European Research Council and Horizon 2020 Grant, Contract Nos. 675440, 724704, 752730, 758316, 765710, 824093, and COST Action CA16108 (European Union); the Leventis Foundation; the Alfred P. Sloan Foundation; the Alexander von Humboldt Foundation; the Science Committee, project no. 22rl-037 (Armenia); the Belgian Federal Science Policy Office; the Fonds pour la Formation à la Recherche dans l'Industrie et dans l'Agriculture (FRIA-Belgium); the Agentschap voor Innovatie door Wetenschap en Technologie (IWT-Belgium); the F.R.S.-FNRS and FWO (Belgium) under the 'Excellence of Science—EOS'—be.h project n. 30820817; the Beijing Municipal Science & Technology Commission, No. Z191100007219010 and Fundamental Research Funds for the Central Universities (China); the Ministry of Education, Youth and Sports (MEYS) of the Czech Republic; the Shota Rustaveli National Science Foundation, Grant FR-22-985 (Georgia); the Deutsche Forschungsgemeinschaft (DFG), under Germany's Excellence Strategy—EXC 2121 'Quantum Universe'—390833306, and under Project Number 400140256—GRK2497; the Hellenic Foundation for Research and Innovation (HFRI), Project Number 2288 (Greece); the Hungarian Academy of Sciences, the New National Excellence Program—ÚNKP, the NKFIH research Grants K 124845, K 124850, K 128713, K 128786, K 129058, K 131991, K 133046, K 138136, K 143460, K 143477, 2020-2.2.1-ED-2021-00181, and TKP2021-NKTA-64 (Hungary); the Council of Science and Industrial Research, India; ICSC—National Research Center for High Performance Computing, Big Data and Quantum Computing, funded by the NextGenerationEU program (Italy); the Latvian Council of Science; the Ministry of Education and Science, Project No. 2022/WK/14, and the National Science Center, contracts Opus 2021/41/B/ST2/01369 and 2021/43/B/ST2/01552 (Poland); the Fundação para a Ciência e a Tecnologia, Grant CEECIND/01334/2018 (Portugal); the National Priorities Research Program by Qatar National Research Fund; MCIN/AEI/10.13039/501100011033, ERDF 'a way of making Europe', and the Programa Estatal de Fomento de la Investigación Científica y Técnica de Excelencia María de Maeztu, Grant MDM-2017-0765 and Programa Severo Ochoa del Principado de Asturias (Spain); the Chulalongkorn Academic into Its 2nd Century Project Advancement Project, and the National Science, Research and Innovation Fund via the Program Management Unit for Human Resources & Institutional Development, Research and Innovation, Grant B37G660013 (Thailand); the Kavli Foundation; the Nvidia Corporation; the SuperMicro Corporation; the Welch Foundation, Contract C-1845; and the Weston Havens Foundation (USA).

Appendix

A.1. Additional figures

In this section, we include auxiliary figures that are omitted from the main body of the paper.

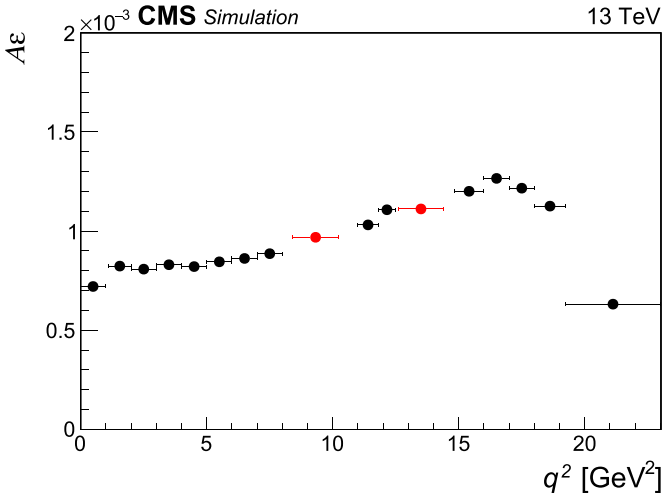

Figure A1. The product of acceptance and efficiency ($\mathcal{A}\epsilon$) of the $B^+ \to K^+\mu^+\mu^-$ channel, as a function of the muon pair q^2, as measured in simulated signal events, after all the corrections applied. Regions corresponding to resonances are displayed with red markers.

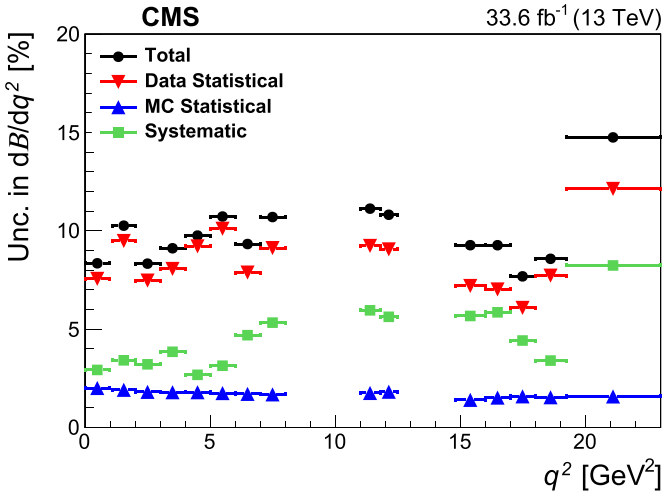

Figure A2. Relative uncertainties in the differential branching fraction measurement of $B^+ \to K^+\mu^+\mu^-$ per q^2 bin. Different colors correspond to data statistical, simulation statistical, and systematic uncertainties.

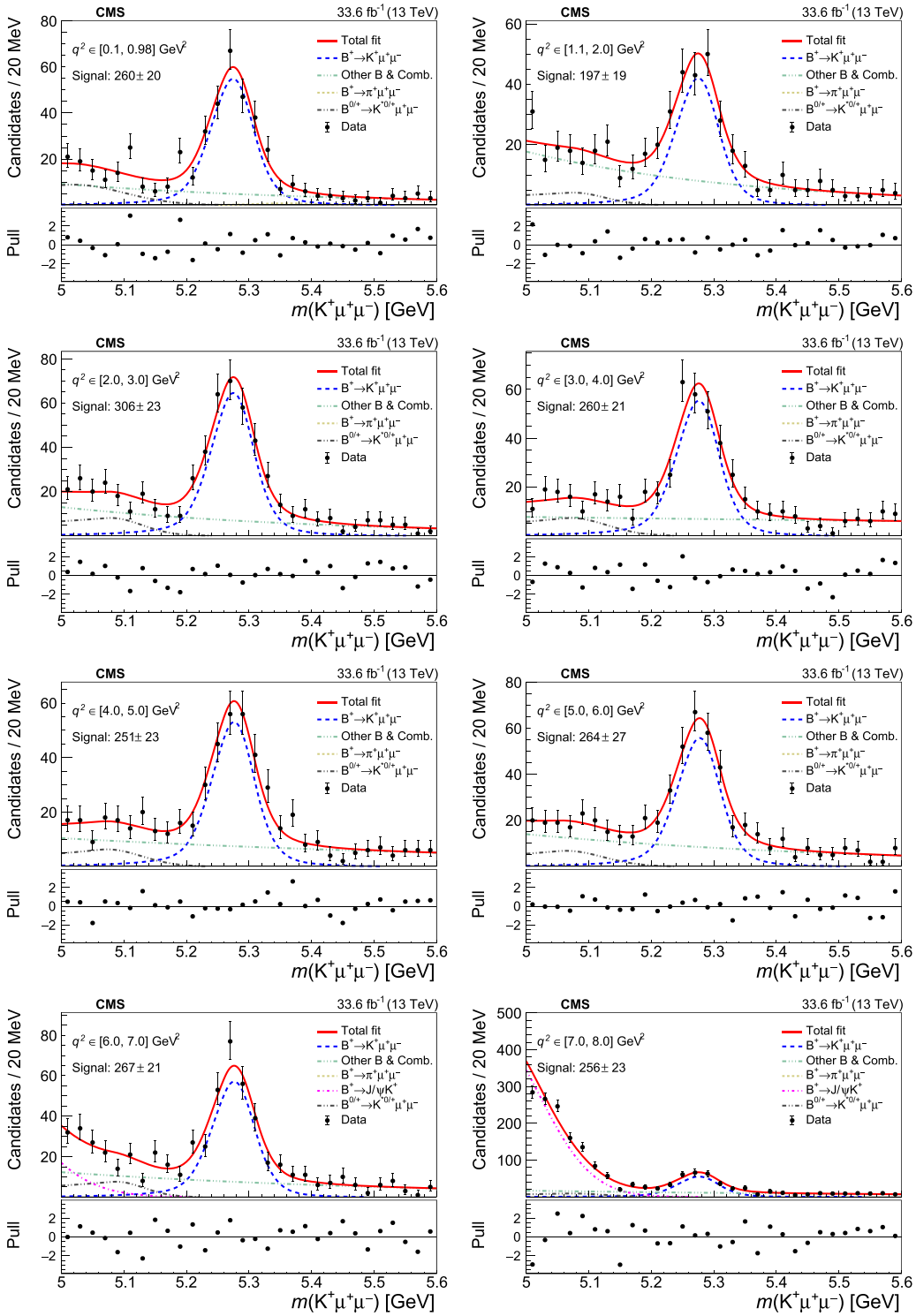

Figure A3. The $K^+\mu^+\mu^-$ invariant mass distributions in various q^2 bins, with the result of the simultaneous fit overlaid in blue and the individual fit components as described in the legends for (from upper left to lower right): $[0, 0.98]$, $[1.1, 2.0]$, $[2.0, 3.0]$ $[3.0, 4.0]$, $[4.0, 5.0]$, $[5.0, 6.0]$, $[6.0, 7.0]$, and $[7.0, 8.0]$, q^2 bins. Notations are as in figure 3.

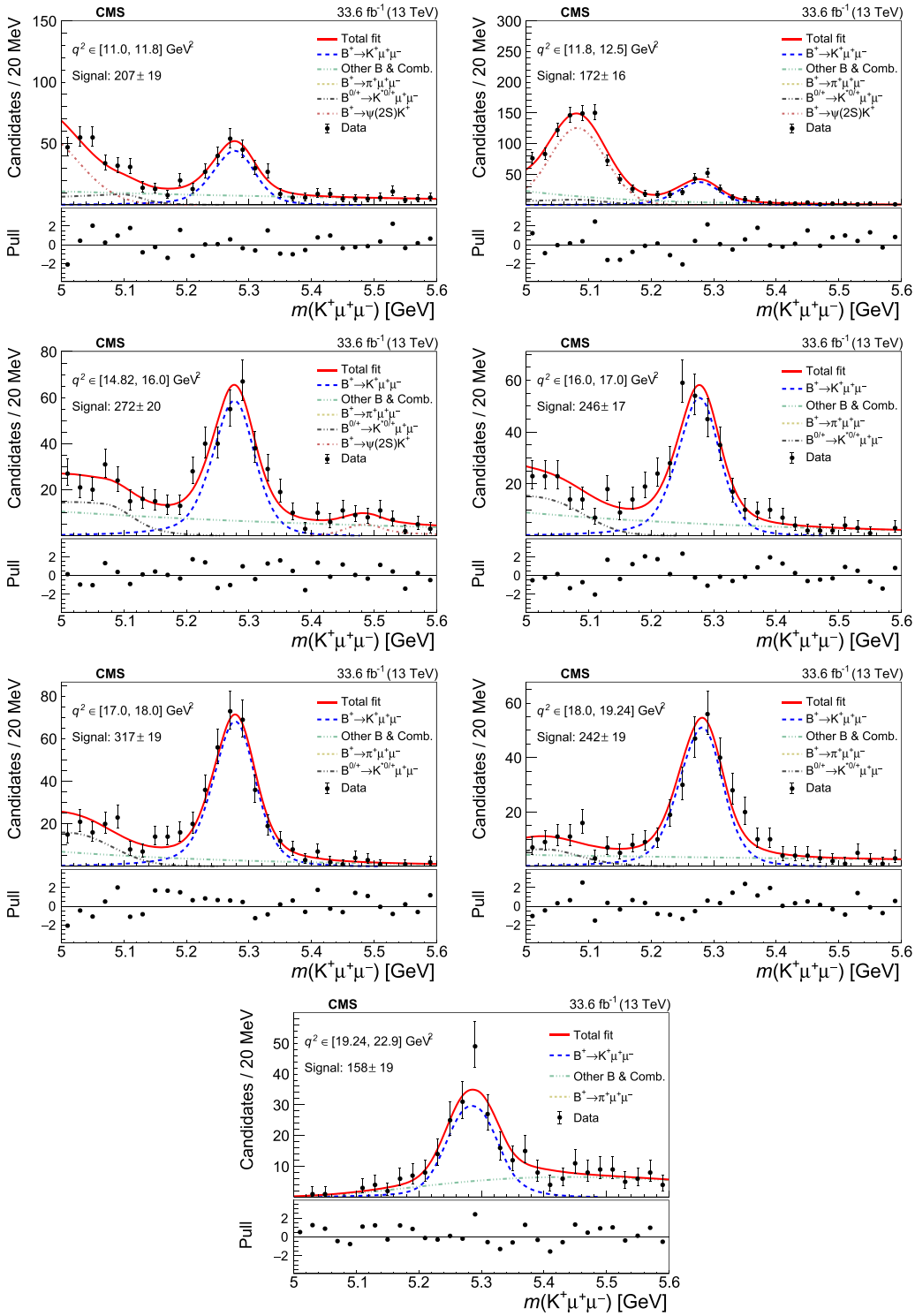

Figure A4. The $K^+\mu^+\mu^-$ invariant mass distributions in various q^2 bins, with the result of the simultaneous fit overlaid in blue and the individual fit components as described in the legends for (from upper left to lower right): $[11.0, 11.8]$, $[11.8, 12.5]$, $[14.82, 16.0]$, $[16.0, 17.0]$, $[17.0, 18.0]$, $[18.0, 19.24]$, and $[19.24, 22.9]\,\mathrm{GeV}^2$ q^2 bins. Notations are as in figure 3.

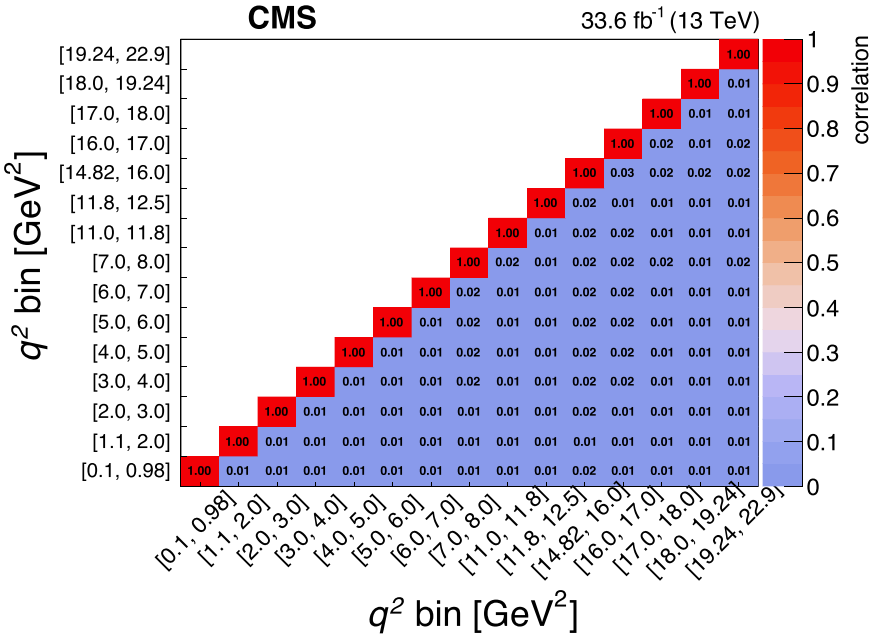

Figure A5. Correlation matrix for the differential branching fraction extraction between different q^2 bins in the simultaneous fit.

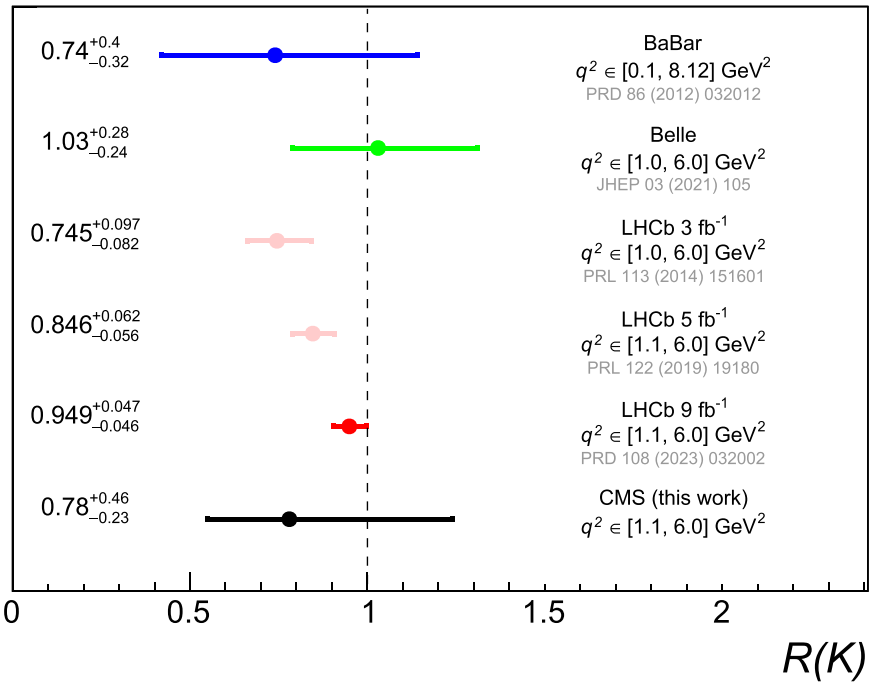

Figure A6. Summary of $R(\mathrm{K})$ measurements from BaBar [12], Belle [15], and LHCb [9, 19, 20] experiments, as well as the present CMS measurement. The pink data points of the first three LHCb measurements were superseded by the latest one, shown as the red point.

A.2. $R(K)$ measurement formalism

The experimentally accessible equivalent of equation (2) can be written as follows, using the event yields N from the fits to the B candidate mass spectra and the products of acceptances and efficiencies ($\mathcal{A}\epsilon\epsilon_{\mathrm{trig}}$ in the muon channel and $\mathcal{A}\epsilon$ in the electron channel):

$$R(\mathrm{K}) = \left(\frac{N_{\mathrm{B}^+\to\mathrm{K}^+\mu^+\mu^-} / N_{\mathrm{B}^+\to\mathrm{J}/\psi(\mu^+\mu^-)\mathrm{K}^+}}{N_{\mathrm{B}^+\to\mathrm{K}^+\mathrm{e}^+\mathrm{e}^-} / N_{\mathrm{B}^+\to\mathrm{J}/\psi(\mathrm{e}^+\mathrm{e}^-)\mathrm{K}^+}} \right) \times \left(\frac{(\mathcal{A}\epsilon)_{\mathrm{B}^+\to\mathrm{K}^+\mathrm{e}^+\mathrm{e}^-} / (\mathcal{A}\epsilon)_{\mathrm{B}^+\to\mathrm{J}/\psi(\mathrm{e}^+\mathrm{e}^-)\mathrm{K}^+}}{(\mathcal{A}\epsilon\epsilon_{\mathrm{trig}})_{\mathrm{B}^+\to\mathrm{K}^+\mu^+\mu^-} / (\mathcal{A}\epsilon\epsilon_{\mathrm{trig}})_{\mathrm{B}^+\to\mathrm{J}/\psi(\mu^+\mu^-)\mathrm{K}^+}} \right). \quad \text{(A.1)}$$

In order to obtain the best fit value of $R(\mathrm{K})$ and its confidence interval, the measured quantities $N_{\mathrm{B}^+\to\mathrm{K}^+\mu^+\mu^-}$ and $N_{\mathrm{B}^+\to\mathrm{K}^+\mathrm{e}^+\mathrm{e}^-}$ are expressed as

$$N_{\mathrm{B}^+\to\mathrm{K}^+\mu^+\mu^-} = R_{\mathcal{B}}\frac{N_{\mathrm{B}^+\to\mathrm{J}/\psi(\mu^+\mu^-)\mathrm{K}^+}}{\mathcal{B}(\mathrm{J}/\psi\to\mu^+\mu^-)}\frac{(\mathcal{A}\epsilon\epsilon_{\mathrm{trig}})_{\mathrm{B}^+\to\mathrm{K}^+\mu^+\mu^-}}{(\mathcal{A}\epsilon\epsilon_{\mathrm{trig}})_{\mathrm{B}^+\to\mathrm{J}/\psi(\mu^+\mu^-)\mathrm{K}^+}} \tag{A.2}$$

and

$$N_{\mathrm{B}^+\to\mathrm{K}^+\mathrm{e}^+\mathrm{e}^-} = R(\mathrm{K})^{-1}R_{\mathcal{B}}\frac{N_{\mathrm{B}^+\to\mathrm{J}/\psi(\mathrm{e}^+\mathrm{e}^-)\mathrm{K}^+}}{\mathcal{B}(\mathrm{J}/\psi\to\mathrm{e}^+\mathrm{e}^-)} \cdot\frac{(\mathcal{A}\epsilon)_{\mathrm{B}^+\to\mathrm{K}^+\mathrm{e}^+\mathrm{e}^-}}{(\mathcal{A}\epsilon)_{\mathrm{B}^+\to\mathrm{J}/\psi(\mathrm{e}^+\mathrm{e}^-)\mathrm{K}^+}}, \tag{A.3}$$

where $R_{\mathcal{B}} = \frac{\mathcal{B}(\mathrm{B}^+\to\mathrm{K}^+\mu^+\mu^-)}{\mathcal{B}(\mathrm{B}^+\to\mathrm{K}^+\mathrm{J}/\psi)}$. We note that $R(\mathrm{K})^{-1}$ is used as the parameter of interest instead of $R(\mathrm{K})$ because this choice makes the likelihood significantly more Gaussian.

A simultaneous fit is done using equations (A.2) and (A.3), with the likelihood function in each lepton channel defined as

$$\begin{aligned}\mathcal{L}^{\mu} = {}& \mathcal{L}^{\mu}_{\text{low-}q^2}\left(N_{\mathrm{B}^+\to\mathrm{K}^+\mu^+\mu^-}\right)\mathcal{L}^{\mu}_{\mathrm{J}/\psi}\left(N_{\mathrm{B}^+\to\mathrm{J}/\psi(\mu^+\mu^-)\mathrm{K}^+}\right)\\ &\times G\left((\mathcal{A}\epsilon\epsilon_{\mathrm{trig}})_{\mathrm{B}^+\to\mathrm{K}^+\mu^+\mu^-}\right)\\ &\times G\left((\mathcal{A}\epsilon\epsilon_{\mathrm{trig}})_{\mathrm{B}^+\to\mathrm{J}/\psi(\mu^+\mu^-)\mathrm{K}^+}\right)G\left(\mathcal{B}^{\mu}_{\mathrm{J}/\psi}\right), \end{aligned}\tag{A.4}$$

$$\begin{aligned}\mathcal{L}^{\mathrm{P}} = {}& \mathcal{L}^{\mathrm{P}}_{\text{low-}q^2}\left(N_{\mathrm{B}^+\to\mathrm{K}^+\mathrm{e}^+\mathrm{e}^-}\right)\mathcal{L}^{\mathrm{P}}_{\mathrm{J}/\psi}\left(N_{\mathrm{B}^+\to\mathrm{J}/\psi(\mathrm{e}^+\mathrm{e}^-)\mathrm{K}^+}\right)\\ &\times G\left((\mathcal{A}\epsilon)_{\mathrm{B}^+\to\mathrm{K}^+\mathrm{e}^+\mathrm{e}^-}\right)\\ &\times G\left((\mathcal{A}\epsilon)_{\mathrm{B}^+\to\mathrm{J}/\psi(\mathrm{e}^+\mathrm{e}^-)\mathrm{K}^+}\right)G\left(\mathcal{B}^{\mathrm{P}}_{\mathrm{J}/\psi}\right), \end{aligned}\tag{A.5}$$

where $\mathcal{L}^{\ell}_{\text{low-}q^2}$ and $\mathcal{L}^{\ell}_{\mathrm{J}/\psi}$ ($\ell = \mu$ or P) are the mass fit likelihood function used in the low-q^2 and J/ψ regions, respectively, G is the Gaussian function with the mean at the nominal value of the argument and the RMS given by the corresponding uncertainty, and $\mathcal{B}^{\ell}_{\mathrm{J}/\psi}$ is the branching fraction of the $\mathrm{J}/\psi\to\ell\ell$ decay. The value of $R(\mathrm{K})$ is measured by maximizing the likelihood function $\mathcal{L} = \mathcal{L}^{\mu}\mathcal{L}^{\mathrm{P}}$, either for a single dielectron category or for the two categories simultaneously, which is achieved by taking $\mathcal{L}^{\mathrm{P}} = \mathcal{L}^{\text{PF-PF}}\mathcal{L}^{\text{PF-LP}}$.

The CMS Collaboration

A Hayrapetyan, A Tumasyan[1]
Yerevan Physics Institute, Yerevan, Armenia

W Adam, J W Andrejkovic, T Bergauer, S Chatterjee, K Damanakis, M Dragicevic, P S Hussain, M Jeitler[2], N Krammer, A Li, D Liko, I Mikulec, J Schieck[2], R Schöfbeck, D Schwarz, M Sonawane, S Templ, W Waltenberger, C -E Wulz[2]
Institut für Hochenergiephysik, Vienna, Austria

M R Darwish[3], T Janssen, P Van Mechelen
Universiteit Antwerpen, Antwerpen, Belgium

E S Bols, J D'Hondt, S Dansana, A De Moor, M Delcourt, H El Faham, S Lowette, I Makarenko, D Müller, A.R Sahasransu, S Tavernier, M Tytgat[4], G.P Van Onsem, S Van Putte, D Vannerom
Vrije Universiteit Brussel, Brussel, Belgium

B Clerbaux, A K Das, G De Lentdecker, L Favart, P Gianneios, D Hohov, J Jaramillo, A Khalilzadeh, K Lee, M Mahdavikhorrami, A Malara, S Paredes, N Postiau, L Thomas, M Vanden Bemden, C Vander Velde, P Vanlaer
Université Libre de Bruxelles, Bruxelles, Belgium

M De Coen, D Dobur, Y Hong, J Knolle, L Lambrecht, G Mestdach, K Mota Amarilo, C Rendón, A Samalan, K Skovpen, N Van Den Bossche, J van der Linden, L Wezenbeek
Ghent University, Ghent, Belgium

A Benecke, A Bethani, G Bruno, C Caputo, C Delaere, I S Donertas, A Giammanco, K Jaffel, Sa Jain, V Lemaitre, J Lidrych, P Mastrapasqua, K Mondal, T T Tran, S Wertz
Université Catholique de Louvain, Louvain-la-Neuve, Belgium

G A Alves, E Coelho, C Hensel, T Menezes De Oliveira, A Moraes, P Rebello Teles, M Soeiro
Centro Brasileiro de Pesquisas Fisicas, Rio de Janeiro, Brazil

W L Aldá Júnior, M Alves Gallo Pereira, M Barroso Ferreira Filho, H Brandao Malbouisson, W Carvalho, J Chinellato[5], E M Da Costa, G G Da Silveira[6], D De Jesus Damiao, S Fonseca De Souza, R Gomes De Souza, J Martins[7], C Mora Herrera, L Mundim, H Nogima, J P Pinheiro, A Santoro, A Sznajder, M Thiel, A Vilela Pereira
Universidade do Estado do Rio de Janeiro, Rio de Janeiro, Brazil

C A Bernardes[6], L Calligaris, T R Fernandez Perez Tomei, E M Gregores, P G Mercadante, S F Novaes, B Orzari, Sandra S Padula
Universidade Estadual Paulista, Universidade Federal do ABC, São Paulo, Brazil

A Aleksandrov, G Antchev, R Hadjiiska, P Iaydjiev, M Misheva, M Shopova, G Sultanov
Institute for Nuclear Research and Nuclear Energy, Bulgarian Academy of Sciences, Sofia, Bulgaria

A Dimitrov, L Litov, B Pavlov, P Petkov, A Petrov, E Shumka
University of Sofia, Sofia, Bulgaria

S Keshri, S Thakur
Instituto De Alta Investigación, Universidad de Tarapacá, Casilla 7 D, Arica, Chile

T Cheng, T Javaid, L Yuan
Beihang University, Beijing, People's Republic of China

Z Hu, J Liu, K Yi[8,9]
Department of Physics, Tsinghua University, Beijing, People's Republic of China

G.M Chen[10], H S Chen[10], M Chen[10], F Iemmi, C H Jiang, A Kapoor[11], H Liao, Z -A Liu[12], R Sharma[13], J N Song[12], J Tao, C Wang[10], J Wang, Z Wang[10], H Zhang
Institute of High Energy Physics, Beijing, People's Republic of China

A Agapitos, Y Ban, A Levin, C Li, Q Li, Y Mao, S J Qian, X Sun, D Wang, H Yang, L Zhang, C Zhou
State Key Laboratory of Nuclear Physics and Technology, Peking University, Beijing, People's Republic of China

Z You
Sun Yat-Sen University, Guangzhou, People's Republic of China

N Lu
University of Science and Technology of People's Republic of China , Hefei, People's Republic of China

G Bauer[14]
Nanjing Normal University, Nanjing, People's Republic of China

X Gao[15], D Leggat, H Okawa
Institute of Modern Physics and Key Laboratory of Nuclear Physics and Ion-beam Application (MOE) - Fudan University, Shanghai, People's Republic of China

Z Lin, C Lu, M Xiao
Zhejiang University, Hangzhou, Zhejiang, People's Republic of China

C Avila, D A Barbosa Trujillo, A Cabrera, C Florez, J Fraga, J A Reyes Vega
Universidad de Los Andes, Bogota, Colombia

J Mejia Guisao, F Ramirez, M Rodriguez, J D Ruiz Alvarez
Universidad de Antioquia, Medellin, Colombia

D Giljanovic, N Godinovic, D Lelas, A Sculac
University of Split, Faculty of Electrical Engineering, Mechanical Engineering and Naval Architecture, Split, Croatia

M Kovac, T Sculac
University of Split, Faculty of Science, Split, Croatia

P Bargassa, V Brigljevic, B K Chitroda, D Ferencek, S Mishra, A Starodumov[16], T Susa
Institute Rudjer Boskovic, Zagreb, Croatia

A Attikis, K Christoforou, S Konstantinou, J Mousa, C Nicolaou, F Ptochos, P A Razis, H Rykaczewski, H Saka, A Stepennov
University of Cyprus, Nicosia, Cyprus

M Finger, M Finger Jr, A Kveton
Charles University, Prague, Czech Republic

E Ayala
Escuela Politecnica Nacional, Quito, Ecuador

E Carrera Jarrin
Universidad San Francisco de Quito, Quito, Ecuador

A A Abdelalim[17,18], E Salama[19,20]
Academy of Scientific Research and Technology of the Arab Republic of Egypt, Egyptian Network of High Energy Physics, Cairo, Egypt

A Lotfy, M A Mahmoud
Center for High Energy Physics (CHEP-FU), Fayoum University, El-Fayoum, Egypt

K Ehataht, M Kadastik, T Lange, S Nandan, C Nielsen, J Pata, M Raidal, L Tani, C Veelken
National Institute of Chemical Physics and Biophysics, Tallinn, Estonia

H Kirschenmann, K Osterberg, M Voutilainen
Department of Physics, University of Helsinki, Helsinki, Finland

S Bharthuar, E Brücken, F Garcia, K T S Kallonen, R Kinnunen, T Lampén, K Lassila-Perini, S Lehti, T Lindén, L Martikainen, M Myllymäki, M m Rantanen, H Siikonen, E Tuominen, J Tuominiemi
Helsinki Institute of Physics, Helsinki, Finland

P Luukka, H Petrow
Lappeenranta-Lahti University of Technology, Lappeenranta, Finland

M Besancon, F Couderc, M Dejardin, D Denegri, J L Faure, F Ferri, S Ganjour, P Gras, G Hamel de Monchenault, V Lohezic, J Malcles, J Rander, A Rosowsky, M.Ö Sahin, A Savoy-Navarro[21], P Simkina, M Titov, M Tornago
IRFU, CEA, Université Paris-Saclay, Gif-sur-Yvette, France

C Baldenegro Barrera, F Beaudette, A Buchot Perraguin, P Busson, A Cappati, C Charlot, M Chiusi, F Damas, O Davignon, A De Wit, B A Fontana Santos Alves, S Ghosh, A Gilbert, R Granier de Cassagnac, A Hakimi, B Harikrishnan, L Kalipoliti, G Liu, J Motta, M Nguyen, C Ochando, L Portales, R Salerno, J B Sauvan, Y Sirois, A Tarabini, E Vernazza, A Zabi, A Zghiche
Laboratoire Leprince-Ringuet, CNRS/IN2P3, Ecole Polytechnique, Institut Polytechnique de Paris, Palaiseau, France

J -L Agram[22], J Andrea, D Apparu, D Bloch, J -M Brom, E.C Chabert, C Collard, S Falke, U Goerlach, C Grimault, R Haeberle, A -C Le Bihan, M Meena, G Saha, M A Sessini, P Van Hove
Université de Strasbourg, CNRS, IPHC UMR 7178, Strasbourg, France

S Beauceron, B Blancon, G Boudoul, N Chanon, J Choi, D Contardo, P Depasse, C Dozen[23], H El Mamouni, J Fay, S Gascon, M Gouzevitch, C Greenberg, G Grenier, B Ille, I B Laktineh, M Lethuillier, L Mirabito, S Perries, A Purohit, M Vander Donckt, P Verdier, J Xiao
Institut de Physique des 2 Infinis de Lyon (IP2I), Villeurbanne, France

D Chokheli, I Lomidze, Z Tsamalaidze[16]
Georgian Technical University, Tbilisi, Georgia

V Botta, L Feld, K Klein, M Lipinski, D Meuser, A Pauls, N Röwert, M Teroerde
RWTH Aachen University, I. Physikalisches Institut, Aachen, Germany

S Diekmann, A Dodonova, N Eich, D Eliseev, F Engelke, J Erdmann, M Erdmann, P Fackeldey, B Fischer, T Hebbeker, K Hoepfner, F Ivone, A Jung, M y Lee, L Mastrolorenzo, F Mausolf, M Merschmeyer, A Meyer, S Mukherjee, D Noll, F Nowotny, A Pozdnyakov, Y Rath, W Redjeb, F Rehm, H Reithler, U Sarkar, V Sarkisovi, A Schmidt, A Sharma, J L Spah, A Stein, F Torres Da Silva De Araujo[24], L Vigilante, S Wiedenbeck, S Zaleski
RWTH Aachen University, III. Physikalisches Institut A, Aachen, Germany

C Dziwok, G Flügge, W Haj Ahmad[25], T Kress, A Nowack, O Pooth, A Stahl, T Ziemons, A Zotz
RWTH Aachen University, III. Physikalisches Institut B, Aachen, Germany

H Aarup Petersen, M Aldaya Martin, J Alimena, S Amoroso, Y An, S Baxter, M Bayatmakou, H Becerril Gonzalez, O Behnke, A Belvedere, S Bhattacharya, F Blekman[26], K Borras[27], A Campbell, A Cardini, C Cheng, F Colombina, S Consuegra Rodríguez, G Correia Silva, M De Silva, G Eckerlin, D Eckstein, L I Estevez Banos, O Filatov, E Gallo[26], A Geiser, A Giraldi, G Greau, V Guglielmi, M Guthoff, A Hinzmann, A Jafari[28], L Jeppe, N Z Jomhari, B Kaech, M Kasemann, C Kleinwort, R Kogler, M Komm, D Krücker, W Lange, D Leyva Pernia, K Lipka[29], W Lohmann[30], R Mankel, I -A Melzer-Pellmann, M Mendizabal Morentin, A B Meyer, G Milella, A Mussgiller, L P Nair, A Nürnberg, Y Otarid, J Park, D Pérez Adán, E Ranken, A Raspereza, B Ribeiro Lopes, J Rübenach, A Saggio, M Scham[31,27], S Schnake[27], P Schütze, C Schwanenberger[26], D Selivanova, K Sharko, M Shchedrolosiev, R E Sosa Ricardo, D Stafford, F Vazzoler, A Ventura Barroso, R Walsh, Q Wang, Y Wen, K Wichmann, L Wiens[27], C Wissing, Y Yang, A Zimermmane Castro Santos
Deutsches Elektronen-Synchrotron, Hamburg, Germany

A Albrecht, S Albrecht, M Antonello, S Bein, L Benato, S Bollweg, M Bonanomi, P Connor, M Eich, K El Morabit, Y Fischer, A Fröhlich, C Garbers, E Garutti, A Grohsjean, M Hajheidari, J Haller, H R Jabusch, G Kasieczka, P Keicher, R Klanner, W Korcari, T Kramer, V Kutzner, F Labe, J Lange, A Lobanov, C Matthies, A Mehta, L Moureaux, M Mrowietz, A Nigamova, Y Nissan, A Paasch, K J Pena Rodriguez, T Quadfasel, B Raciti, M Rieger, D Savoiu, J Schindler, P Schleper, M Schröder, J Schwandt, M Sommerhalder, H Stadie, G Steinbrück, A Tews, M Wolf
University of Hamburg, Hamburg, Germany

S Brommer, M Burkart, E Butz, T Chwalek, A Dierlamm, A Droll, N Faltermann, M Giffels, A Gottmann, F Hartmann[32], R Hofsaess, M Horzela, U Husemann, J Kieseler, M Klute, R Koppenhöfer, J M Lawhorn, M Link, A Lintuluoto, S Maier, S Mitra, M Mormile, Th Müller, M Neukum, M Oh, M Presilla, G Quast, K Rabbertz, B Regnery, N Shadskiy, I Shvetsov, H J Simonis, M Toms, N Trevisani, R Ulrich, R F Von Cube, M Wassmer, S Wieland, F Wittig, R Wolf, X Zuo
Karlsruher Institut fuer Technologie, Karlsruhe, Germany

G Anagnostou, G Daskalakis, A Kyriakis, A Papadopoulos[32], A Stakia
Institute of Nuclear and Particle Physics (INPP), NCSR Demokritos, Aghia Paraskevi, Greece

P Kontaxakis, G Melachroinos, A Panagiotou, I Papavergou, I Paraskevas, N Saoulidou, K Theofilatos, E Tziaferi, K Vellidis, I Zisopoulos
National and Kapodistrian University of Athens, Athens, Greece

G Bakas, T Chatzistavrou, G Karapostoli, K Kousouris, I Papakrivopoulos, E Siamarkou, G Tsipolitis, A Zacharopoulou
National Technical University of Athens, Athens, Greece

K Adamidis, I Bestintzanos, I Evangelou, C Foudas, C Kamtsikis, P Katsoulis, P Kokkas, P G Kosmoglou Kioseoglou, N Manthos, I Papadopoulos, J Strologas
University of Ioánnina, Ioánnina, Greece

M Bartók[33], C Hajdu, D Horvath[34,35], K Márton, F Sikler, V Veszpremi
HUN-REN Wigner Research Centre for Physics, Budapest, Hungary

M Csanád, K Farkas, M M A Gadallah[36], Á Kadlecsik, P Major, K Mandal, G Pásztor, A.J Rádl[37], G.I Veres
MTA-ELTE Lendület CMS Particle and Nuclear Physics Group, Eötvös Loránd University, Budapest, Hungary

P Raics, B Ujvari, G Zilizi
Faculty of Informatics, University of Debrecen, Debrecen, Hungary

G Bencze, S Czellar, J Molnar, Z Szillasi
Institute of Nuclear Research ATOMKI, Debrecen, Hungary

T Csorgo[37], F Nemes[37], T Novak
Karoly Robert Campus, MATE Institute of Technology, Gyongyos, Hungary

J Babbar, S Bansal, S.B Beri, V Bhatnagar, G Chaudhary, S Chauhan, N Dhingra[38], A Kaur, A Kaur, H Kaur, M Kaur, S Kumar, K Sandeep, T Sheokand, J B Singh, A Singla
Panjab University, Chandigarh, India

A Ahmed, A Bhardwaj, A Chhetri, B C Choudhary, A Kumar, A Kumar, M Naimuddin, K Ranjan, S Saumya
University of Delhi, Delhi, India

S Baradia, S Barman[39], S Bhattacharya, S Dutta, S Dutta, S Sarkar
Saha Institute of Nuclear Physics, HBNI, Kolkata, India

M M Ameen, P K Behera, S C Behera, S Chatterjee, P Jana, P Kalbhor, J R Komaragiri[40], D Kumar[40], L Panwar[40], P R Pujahari, N R Saha, A Sharma, A K Sikdar, S Verma
Indian Institute of Technology Madras, Madras, India

S Dugad, M Kumar, G B Mohanty, P Suryadevara
Tata Institute of Fundamental Research-A, Mumbai, India

A Bala, S Banerjee, R M Chatterjee, R K Dewanjee[41], M Guchait, Sh Jain, A Jaiswal, S Karmakar, S Kumar, G Majumder, K Mazumdar, S Parolia, A Thachayath
Tata Institute of Fundamental Research-B, Mumbai, India

S Bahinipati[42], C Kar, D Maity[43], P Mal, T Mishra, V K Muraleedharan Nair Bindhu[43], K Naskar[43], A Nayak[43], P Sadangi, P Saha, S K Swain, S Varghese[43], D Vats[43]
National Institute of Science Education and Research, An OCC of Homi Bhabha National Institute, Bhubaneswar, Odisha, India

S Acharya[44], A Alpana, S Dube, B Gomber[44], B Kansal, A Laha, B Sahu[44], S Sharma, K Y Vaish
Indian Institute of Science Education and Research (IISER), Pune, India

H Bakhshiansohi[45], E Khazaie[46], M Zeinali[47]
Isfahan University of Technology, Isfahan, Iran

S Chenarani[48], S M Etesami, M Khakzad, M Mohammadi Najafabadi
Institute for Research in Fundamental Sciences (IPM), Tehran, Iran

M Grunewald
University College Dublin, Dublin, Ireland

M Abbrescia[a,b], R Aly[a,c,17], A Colaleo[a,b], D Creanza[a,c], B D'Anzi[a,b], N De Filippis[a,c], M De Palma[a,b], A Di Florio[a,c], W Elmetenawee[a,b,17], L Fiore[a], G Iaselli[a,c], M Louka[a,b], G Maggi[a,c], M Maggi[a], I Margjeka[a,b], V Mastrapasqua[a,b], S My[a,b], S Nuzzo[a,b], A Pellecchia[a,b], A Pompili[a,b], G Pugliese[a,c], R Radogna[a], G Ramirez-Sanchez[a,c], D Ramos[a], A Ranieri[a], L Silvestris[a], F M Simone[a,b], Ü Sözbilir[a], A Stamerra[a], R Venditti[a], P Verwilligen[a], A Zaza[a,b]
INFN Sezione di Bari[a], Università di Bari[b], Politecnico di Bari[c], Bari, Italy

G Abbiendi[a], C Battilana[a,b], D Bonacorsi[a,b], L Borgonovi[a], R Campanini[a,b], P Capiluppi[a,b], A Castro[a,b], F R Cavallo[a], M Cuffiani[a,b], T Diotalevi[a,b], F Fabbri[a], A Fanfani[a,b], D Fasanella[a,b], P Giacomelli[a], L Giommi[a,b], C Grandi[a], L Guiducci[a,b], S Lo Meo[a,49], L Lunerti[a,b], S Marcellini[a], G Masetti[a], F L

Navarria[a,b], A Perrotta[a], F Primavera[a,b], A M Rossi[a,b], T Rovelli[a,b], G P Siroli[a,b]
INFN Sezione di Bologna[a], Università di Bologna[b], Bologna, Italy

S Costa[a,b,50], A Di Mattia[a], R Potenza[a,b], A Tricomi[a,b,50], C Tuve[a,b]
INFN Sezione di Catania[a], Università di Catania[b], Catania, Italy

P Assiouras[a], G Barbagli[a], G Bardelli[a,b], B Camaiani[a,b], A Cassese[a], R Ceccarelli[a], V Ciulli[a,b], C Civinini[a], R D'Alessandro[a,b], E Focardi[a,b], T Kello[a], G Latino[a,b], P Lenzi[a,b], M Lizzo[a], M Meschini[a], S Paoletti[a], A Papanastassiou[a,b], G Sguazzoni[a], L Viliani[a]
INFN Sezione di Firenze[a], Università di Firenze[b], Firenze, Italy

L Benussi, S Bianco, S Meola[51], D Piccolo
INFN Laboratori Nazionali di Frascati, Frascati, Italy

P Chatagnon[a], F Ferro[a], E Robutti[a], S Tosi[a,b]
INFN Sezione di Genova[a], Università di Genova[b], Genova, Italy

A Benaglia[a], G Boldrini[a,b], F Brivio[a], F Cetorelli[a], F De Guio[a,b], M E Dinardo[a,b], P Dini[a], S Gennai[a], R Gerosa[a,b], A Ghezzi[a,b], P Govoni[a,b], L Guzzi[a], M T Lucchini[a,b], M Malberti[a], S Malvezzi[a], A Massironi[a], D Menasce[a], L Moroni[a], M Paganoni[a,b], D Pedrini[a], B S Pinolini[a], S Ragazzi[a,b], T Tabarelli de Fatis[a,b], D Zuolo[a]
INFN Sezione di Milano-Bicocca[a], Università di Milano-Bicocca[b], Milano, Italy

S Buontempo[a], A Cagnotta[a,b], F Carnevali[a,b], N Cavallo[a,c], F Fabozzi[a,c], A O M Iorio[a,b], L Lista[a,b,52], P Paolucci[a,32], B Rossi[a], C Sciacca[a,b]
INFN Sezione di Napoli[a], Università di Napoli 'Federico II'[b], Napoli, Italy; Università della Basilicata[c], Potenza, Italy; Scuola Superiore Meridionale (SSM)[d], Napoli, Italy

R Ardino[a], P Azzi[a], N Bacchetta[a,53], P Bortignon[a], A Bragagnolo[a,b], R Carlin[a,b], P Checchia[a], T Dorigo[a], F Gasparini[a,b], U Gasparini[a,b], E Lusiani[a], M Margoni[a,b], F Marini[a], A T Meneguzzo[a,b], M Migliorini[a,b], F Montecassiano[a], J Pazzini[a,b], P Ronchese[a,b], R Rossin[a,b], F Simonetto[a,b], G Strong[a], M Tosi[a,b], A Triossi[a,b], S Ventura[a], H Yarar[a,b], M Zanetti[a,b], P Zotto[a,b], A Zucchetta[a,b], G Zumerle[a,b]
INFN Sezione di Padova[a], Università di Padova[b], Padova, Italy; Università di Trento[c], Trento, Italy

S Abu Zeid[a,20], C Aimè[a,b], A Braghieri[a], S Calzaferri[a], D Fiorina[a], P Montagna[a,b], V Re[a], C Riccardi[a,b], P Salvini[a], I Vai[a,b], P Vitulo[a,b]
INFN Sezione di Pavia[a], Università di Pavia[b], Pavia, Italy

S Ajmal[a,b], G M Bilei[a], D Ciangottini[a,b], L Fanò[a,b], M Magherini[a,b], G Mantovani[a,b], V Mariani[a,b], M Menichelli[a], F Moscatelli[a,54], A Rossi[a,b], A Santocchia[a,b], D Spiga[a], T Tedeschi[a,b]
INFN Sezione di Perugia[a], Università di Perugia[b], Perugia, Italy

P Asenov[a,b], P Azzurri[a], G Bagliesi[a], R Bhattacharya[a], L Bianchini[a,b], T Boccali[a], E Bossini[a], D Bruschini[a,c], R Castaldi[a], M A Ciocci[a,b], M Cipriani[a,b], V D'Amante[a,d], R Dell'Orso[a], S Donato[a], A Giassi[a], F Ligabue[a,c], D Matos Figueiredo[a], A Messineo[a,b], M Musich[a,b], F Palla[a], A Rizzi[a,b], G Rolandi[a,c], S Roy Chowdhury[a], T Sarkar[a], A Scribano[a], P Spagnolo[a], R Tenchini[a], G Tonelli[a,b], N Turini[a,d], A Venturi[a], P G Verdini[a]
INFN Sezione di Pisa[a], Università di Pisa[b], Scuola Normale Superiore di Pisa[c], Pisa, Italy; Università di Siena[d], Siena, Italy

P Barria[a], M Campana[a,b], F Cavallari[a], L Cunqueiro Mendez[a,b], D Del Re[a,b], E Di Marco[a], M Diemoz[a], F Errico[a,b], E Longo[a,b], P Meridiani[a], J Mijuskovic[a,b], G Organtini[a,b], F Pandolfi[a], R Paramatti[a,b], C Quaranta[a,b], S Rahatlou[a,b], C Rovelli[a], F Santanastasio[a,b], L Soffi[a]
INFN Sezione di Roma[a], Sapienza Università di Roma[b], Roma, Italy

N Amapane[a,b], R Arcidiacono[a,c], S Argiro[a,b], M Arneodo[a,c], N Bartosik[a], R Bellan[a,b], A Bellora[a,b], C Biino[a], C Borca[a,b], N Cartiglia[a], M Costa[a,b], R Covarelli[a,b], N Demaria[a], L Finco[a], M Grippo[a,b], B Kiani[a,b], F Legger[a], F Luongo[a,b], C Mariotti[a], L Markovic[a,b], S Maselli[a], A Mecca[a,b], E Migliore[a,b], M Monteno[a], R Mulargia[a], M M Obertino[a,b], G Ortona[a], L Pacher[a,b], N Pastrone[a], M Pelliccioni[a], M Ruspa[a,c], F Siviero[a,b], V Sola[a,b], A Solano[a,b], A Staiano[a], C Tarricone[a,b], D Trocino[a], G Umoret[a,b], E Vlasov[a,b]
INFN Sezione di Torino[a], Università di Torino[b], Torino, Italy; Università del Piemonte Orientale[c], Novara, Italy

S Belforte[a], V Candelise[a,b], M Casarsa[a], F Cossutti[a], K De Leo[a,b], G Della Ricca[a,b]
INFN Sezione di Trieste[a], Università di Trieste[b], Trieste, Italy

S Dogra, J Hong, C Huh, B Kim, D.H Kim, J Kim, H Lee, S.W Lee, C.S Moon, Y.D Oh, M.S Ryu, S Sekmen, Y.C Yang
Kyungpook National University, Daegu, Republic of Korea

M S Kim
Department of Mathematics and Physics - GWNU, Gangneung, Republic of Korea

G Bak, P Gwak, H Kim, D H Moon
Chonnam National University, Institute for Universe and Elementary Particles, Kwangju, Republic of Korea

E Asilar, D Kim, T J Kim, J A Merlin
Hanyang University, Seoul, Republic of Korea

S Choi, S Han, B Hong, K Lee, K S Lee, S Lee, J Park, S K Park, J Yoo
Republic of Korea University, Seoul, Republic of Korea

J Goh, S Yang
Kyung Hee University, Department of Physics, Seoul, Republic of Korea

H S Kim, Y Kim, S Lee
Sejong University, Seoul, Republic of Korea

J Almond, J H Bhyun, J Choi, W Jun, J Kim, S Ko, H Kwon, H Lee, J Lee, J Lee, B H Oh, S B Oh, H Seo, U K Yang, I Yoon
Seoul National University, Seoul, Republic of Korea

W Jang, D Y Kang, Y Kang, S Kim, B Ko, J S H Lee, Y Lee, I C Park, Y Roh, I.J Watson
University of Seoul, Seoul, Republic of Korea

S Ha, H D Yoo
Yonsei University, Department of Physics, Seoul, Republic of Korea

M Choi, M R Kim, H Lee, Y Lee, I Yu
Sungkyunkwan University, Suwon, Republic of Korea

T Beyrouthy, Y Maghrbi
College of Engineering and Technology, American University of the Middle East (AUM), Dasman, Kuwait

K Dreimanis, A Gaile, G Pikurs, A Potrebko, M Seidel, V Veckalns[55]
Riga Technical University, Riga, Latvia

N R Strautnieks
University of Latvia (LU), Riga, Latvia

M Ambrozas, A Juodagalvis, A Rinkevicius, G Tamulaitis
Vilnius University, Vilnius, Lithuania

N Bin Norjoharuddeen, I Yusuff[56], Z Zolkapli
National Centre for Particle Physics, Universiti Malaya, Kuala Lumpur, Malaysia

J F Benitez, A Castaneda Hernandez, H A Encinas Acosta, L G Gallegos Maríñez, M León Coello, J A Murillo Quijada, A Sehrawat, L Valencia Palomo
Universidad de Sonora (UNISON), Hermosillo, Mexico

G Ayala, H Castilla-Valdez, H Crotte Ledesma, E De La Cruz-Burelo, I Heredia-De La Cruz[57], R Lopez-Fernandez, C A Mondragon Herrera, A Sánchez Hernández
Centro de Investigacion y de Estudios Avanzados del IPN, Mexico City, Mexico

C Oropeza Barrera, M Ramírez García
Universidad Iberoamericana, Mexico City, Mexico

I Bautista, I Pedraza, H A Salazar Ibarguen, C Uribe Estrada
Benemerita Universidad Autonoma de Puebla, Puebla, Mexico

I Bubanja, N Raicevic
University of Montenegro, Podgorica, Montenegro

P H Butler
University of Canterbury, Christchurch, New Zealand

A Ahmad, M I Asghar, A Awais, M I M Awan, H R Hoorani, W A Khan
National Centre for Physics, Quaid-I-Azam University, Islamabad, Pakistan

V Avati, L Grzanka, M Malawski
AGH University of Krakow, Faculty of Computer Science, Electronics and Telecommunications, Krakow, Poland

H Bialkowska, M Bluj, B Boimska, M Górski, M Kazana, M Szleper, P Zalewski
National Centre for Nuclear Research, Swierk, Poland

K Bunkowski, K Doroba, A Kalinowski, M Konecki, J Krolikowski, A Muhammad
Institute of Experimental Physics, Faculty of Physics, University of Warsaw, Warsaw, Poland

K Pozniak, W Zabolotny
Warsaw University of Technology, Warsaw, Poland

M Araujo, D Bastos, C Beirão Da Cruz E Silva, A Boletti, M Bozzo, T Camporesi, G Da Molin, P Faccioli, M Gallinaro, J Hollar, N Leonardo, T Niknejad, A Petrilli, M Pisano, J Seixas, J Varela, J W Wulff
Laboratório de Instrumentação e Física Experimental de Partículas, Lisboa, Portugal

P Adzic, P Milenovic
Faculty of Physics, University of Belgrade, Belgrade, Serbia

M Dordevic, J Milosevic, V Rekovic
VINCA Institute of Nuclear Sciences, University of Belgrade, Belgrade, Serbia

M Aguilar-Benitez, J Alcaraz Maestre, Cristina F Bedoya, M Cepeda, M Cerrada, N Colino, B De La Cruz, A Delgado Peris, A Escalante Del Valle, D Fernández Del Val, J P Fernández Ramos, J Flix, M C Fouz, O Gonzalez Lopez, S Goy Lopez, J M Hernandez, M I Josa, D Moran, C M Morcillo Perez, Á Navarro Tobar, C Perez Dengra, A Pérez-Calero Yzquierdo, J Puerta Pelayo, I Redondo, D D Redondo Ferrero, L Romero, S Sánchez Navas, L Urda Gómez, J Vazquez Escobar, C Willmott
Centro de Investigaciones Energéticas Medioambientales y Tecnológicas (CIEMAT), Madrid, Spain

J F de Trocóniz
Universidad Autónoma de Madrid, Madrid, Spain

B Alvarez Gonzalez, J Cuevas, J Fernandez Menendez, S Folgueras, I Gonzalez Caballero, J R González Fernández, E Palencia Cortezon, C Ramón Álvarez, V Rodríguez Bouza, A Soto Rodríguez, A Trapote, C Vico Villalba, P Vischia
Universidad de Oviedo, Instituto Universitario de Ciencias y Tecnologías Espaciales de Asturias (ICTEA), Oviedo, Spain

S Bhowmik, S Blanco Fernández, J A Brochero Cifuentes, I J Cabrillo, A Calderon, J Duarte Campderros, M Fernandez, G Gomez, C Lasaosa García, C Martinez Rivero, P Martinez Ruiz del Arbol, F Matorras, P Matorras Cuevas, E Navarrete Ramos, J Piedra Gomez, L Scodellaro, I Vila, J M Vizan Garcia
Instituto de Física de Cantabria (IFCA), CSIC-Universidad de Cantabria, Santander, Spain

M K Jayananda, B Kailasapathy[58], D U J Sonnadara, D D C Wickramarathna
University of Colombo, Colombo, Sri Lanka

W G D Dharmaratna[59], K Liyanage, N Perera, N Wickramage
University of Ruhuna, Department of Physics, Matara, Sri Lanka

D Abbaneo, C Amendola, E Auffray, G Auzinger, J Baechler, D Barney, A Bermúdez Martínez, M Bianco, B Bilin, A A Bin Anuar, A Bocci, C Botta, E Brondolin, C Caillol, G Cerminara, N Chernyavskaya, D d'Enterria, A Dabrowski, A David, A De Roeck, M M Defranchis, M Deile, M Dobson, L Forthomme, G Franzoni, W Funk, S Giani, D Gigi, K Gill, F Glege, L Gouskos, M Haranko, J Hegeman, B Huber, V Innocente, T James, P Janot, S Laurila, P Lecoq, E Leutgeb, C Lourenço, B Maier, L Malgeri, M Mannelli, A C Marini, M Matthewman, F Meijers, S Mersi, E Meschi, V Milosevic, F Monti, F Moortgat, M Mulders, I Neutelings, S Orfanelli, F Pantaleo, G Petrucciani, A Pfeiffer, M Pierini, D Piparo, H Qu, D Rabady, G Reales Gutiérrez, M Rovere, H Sakulin, S Scarfi, C Schwick, M Selvaggi, A Sharma, K Shchelina, P Silva, P Sphicas[60], A G Stahl Leiton, A Steen, S Summers, D Treille, P Tropea, A Tsirou, D Walter, J Wanczyk[61], J Wang, S Wuchterl, P Zehetner, P Zejdl, W D Zeuner
CERN, European Organization for Nuclear Research, Geneva, Switzerland

T Bevilacqua[62], L Caminada[62], A Ebrahimi, W Erdmann, R Horisberger, Q Ingram, H C Kaestli, D Kotlinski, C Lange, M Missiroli[62], L Noehte[62], T Rohe
Paul Scherrer Institut, Villigen, Switzerland

T K Aarrestad, K Androsov[61], M Backhaus, A Calandri, C Cazzaniga, K Datta, A De Cosa, G Dissertori, M Dittmar, M Donegà, F Eble, M Galli, K Gedia, F Glessgen, C Grab, D Hits, W Lustermann, A -M Lyon, R A Manzoni, M Marchegiani, L Marchese, C Martin Perez, A Mascellani[61], F Nessi-Tedaldi, F Pauss, V Perovic, S Pigazzini, C Reissel, T Reitenspiess, B Ristic, F Riti, D Ruini, R Seidita, J Steggemann[61], D Valsecchi, R Wallny
ETH Zurich - Institute for Particle Physics and Astrophysics (IPA), Zurich, Switzerland

C Amsler[63], P Bärtschi, D Brzhechko, M.F Canelli, K Cormier, J K Heikkilä, M Huwiler, W Jin, A Jofrehei, B Kilminster, S Leontsinis, S P Liechti, A Macchiolo, P Meiring, U Molinatti, A Reimers, P Robmann, S Sanchez Cruz, M Senger, Y Takahashi, R Tramontano
Universität Zürich, Zurich, Switzerland

C Adloff[64], D Bhowmik, C M Kuo, W Lin, P K Rout, P C Tiwari[40], S S Yu
National Central University, Chung-Li, Taiwan

L Ceard, Y Chao, K F Chen, P s Chen, Z g Chen, A De Iorio, W -S Hou, T h Hsu, Y w Kao, R Khurana, G Kole, Y y Li, R -S Lu, E Paganis, X f Su, J Thomas-Wilsker, L s Tsai, H y Wu, E Yazgan
National Taiwan University (NTU), Taipei, Taiwan

C Asawatangtrakuldee, N Srimanobhas, V Wachirapusitanand
High Energy Physics Research Unit, Department of Physics, Faculty of Science, Chulalongkorn University, Bangkok, Thailand

D Agyel, F Boran, Z S Demiroglu, F Dolek, I Dumanoglu[65], E Eskut, Y Guler[66], E Gurpinar Guler[66], C Isik, O Kara, A Kayis Topaksu, U Kiminsu, G Onengut, K Ozdemir[67], A Polatoz, B Tali[68], U G Tok, S Turkcapar, E Uslan, I S Zorbakir
Çukurova University, Physics Department, Science and Art Faculty, Adana, Turkey

M Yalvac[69]
Middle East Technical University, Physics Department, Ankara, Turkey

B Akgun, I O Atakisi, E Gülmez, M Kaya[70], O Kaya[71], S Tekten[72]
Bogazici University, Istanbul, Turkey

A Cakir, K Cankocak[65,73], Y Komurcu, S Sen[74]
Istanbul Technical University, Istanbul, Turkey

O Aydilek, S Cerci[68], V Epshteyn, B Hacisahinoglu, I Hos[75], B Kaynak, S Ozkorucuklu, O Potok, H Sert, C Simsek, C Zorbilmez
Istanbul University, Istanbul, Turkey

B Isildak[76], D Sunar Cerci[68]
Yildiz Technical University, Istanbul, Turkey

A Boyaryntsev, B Grynyov
Institute for Scintillation Materials of National Academy of Science of Ukraine, Kharkiv, Ukraine

L Levchuk
National Science Centre, Kharkiv Institute of Physics and Technology, Kharkiv, Ukraine

D Anthony, J J Brooke, A Bundock, F Bury, E Clement, D Cussans, H Flacher, M Glowacki, J Goldstein, H F Heath, L Kreczko, S Paramesvaran, L Robertshaw, S Seif El Nasr-Storey, V J Smith, N Stylianou[77], K Walkingshaw Pass, R White
University of Bristol, Bristol, United Kingdom

A H Ball, K W Bell, A Belyaev[78], C Brew, R M Brown, D J A Cockerill, C Cooke, K V Ellis, K Harder, S Harper, M -L Holmberg[79], J Linacre, K Manolopoulos, D M Newbold, E Olaiya, D Petyt, T Reis, G Salvi, T Schuh, C H Shepherd-Themistocleous, I R Tomalin, T Williams
Rutherford Appleton Laboratory, Didcot, United Kingdom

R Bainbridge, P Bloch, C E Brown, O Buchmuller, V Cacchio, C A Carrillo Montoya, G S Chahal[80], D Colling, J S Dancu, I Das, P Dauncey, G Davies, J Davies, M Della Negra, S Fayer, G Fedi, G Hall, M H Hassanshahi, A Howard, G Iles, M Knight, J Langford, J León Holgado, L Lyons, A -M Magnan, S Malik, M Mieskolainen, J Nash[81], M Pesaresi, B C Radburn-Smith, A Richards, A Rose, K Savva, C Seez, R Shukla, A Tapper, K Uchida, G P Uttley, L H Vage, T Virdee[32], M Vojinovic, N Wardle, D Winterbottom
Imperial College, London, United Kingdom

K Coldham, J E Cole, A Khan, P Kyberd, I D Reid
Brunel University, Uxbridge, United Kingdom

S Abdullin, A Brinkerhoff, B Caraway, J Dittmann, K Hatakeyama, J Hiltbrand, B McMaster, M Saunders, S Sawant, C Sutantawibul, J Wilson
Baylor University, Waco, Texas, United States of America

R Bartek, A Dominguez, C Huerta Escamilla, A E Simsek, R Uniyal, A M Vargas Hernandez
Catholic University of America, Washington, DC, United States of America

B Bam, R Chudasama, S I Cooper, S V Gleyzer, C U Perez, P Rumerio[82], E United States of Americai, R Yi
The University of Alabama, Tuscaloosa, Alabama, United States of America

A Akpinar, D Arcaro, C Cosby, Z Demiragli, C Erice, C Fangmeier, C Fernandez Madrazo, E Fontanesi, D Gastler, F Golf, S Jeon, I Reed, J Rohlf, K Salyer, D Sperka, D Spitzbart, I Suarez, A Tsatsos, S Yuan, A G Zecchinelli
Boston University, Boston, Massachusetts, United States of America

G Benelli, X Coubez[27], D Cutts, M Hadley, U Heintz, J M Hogan[83], T Kwon, G Landsberg, K T Lau, D Li, J Luo, S Mondal, M Narain[†], N Pervan, S Sagir[84], F Simpson, M Stamenkovic, W Y Wong, X Yan, W Zhang
Brown University, Providence, Rhode Island, United States of America

S Abbott, J Bonilla, C Brainerd, R Breedon, M Calderon De La Barca Sanchez, M Chertok, M Citron, J Conway, P.T Cox, R Erbacher, F Jensen, O Kukral, G Mocellin, M Mulhearn, D Pellett, W Wei, Y Yao, F Zhang
University of California, Davis, Davis, California, United States of America

M Bachtis, R Cousins, A Datta, G Flores Avila, J Hauser, M Ignatenko, M A Iqbal, T Lam, E Manca, A Nunez Del Prado, D Saltzberg, V Valuev
University of California, Los Angeles, California, United States of America

R Clare, J W Gary, M Gordon, G Hanson, W Si, S Wimpenny†
University of California, Riverside, Riverside, California, United States of America

J.G Branson, S Cittolin, S Cooperstein, D Diaz, J Duarte, L Giannini, J Guiang, R Kansal, V Krutelyov, R Lee, J Letts, M Masciovecchio, F Mokhtar, S Mukherjee, M Pieri, M Quinnan, B V Sathia Narayanan, V Sharma, M Tadel, E Vourliotis, F Würthwein, Y Xiang, A Yagil
University of California, San Diego, La Jolla, California, United States of America

A Barzdukas, L Brennan, C Campagnari, A Dorsett, J Incandela, J Kim, A J Li, P Masterson, H Mei, J Richman, U Sarica, R Schmitz, F Setti, J Sheplock, D Stuart, T Á Vámi, S Wang
University of California, Santa Barbara - Department of Physics, Santa Barbara, California, United States of America

A Bornheim, O Cerri, A Latorre, J Mao, H B Newman, M Spiropulu, J.R Vlimant, C Wang, S Xie, R.Y Zhu
California Institute of Technology, Pasadena, California, United States of America

J Alison, S An, M B Andrews, P Bryant, M Cremonesi, V Dutta, T Ferguson, A Harilal, C Liu, T Mudholkar, S Murthy, P Palit, M Paulini, A Roberts, A Sanchez, W Terrill
Carnegie Mellon University, Pittsburgh, Pennsylvania, United States of America

J P Cumalat, W T Ford, A Hart, A Hassani, G Karathanasis, E MacDonald, N Manganelli, A Perloff, C Savard, N Schonbeck, K Stenson, K A Ulmer, S R Wagner, N Zipper
University of Colorado Boulder, Boulder, Colorado, United States of America

J Alexander, S Bright-Thonney, X Chen, D J Cranshaw, J Fan, X Fan, D Gadkari, S Hogan, P Kotamnives, J Monroy, M Oshiro, J R Patterson, J Reichert, M Reid, A Ryd, J Thom, P Wittich, R Zou
Cornell University, Ithaca, New York, United States of America

M Albrow, M Alyari, O Amram, G Apollinari, A Apresyan, L A T Bauerdick, D Berry, J Berryhill, P C Bhat, K Burkett, J N Butler, A Canepa, G B Cerati, H W K Cheung, F Chlebana, G Cummings, J Dickinson, I Dutta, V D Elvira, Y Feng, J Freeman, A Gandrakota, Z Gecse, L Gray, D Green, A Grummer, S Grünendahl, D Guerrero, O Gutsche, R M Harris, R Heller, T C Herwig, J Hirschauer, L Horyn, B Jayatilaka, S Jindariani, M Johnson, U Joshi, T Klijnsma, B Klima, K H.M Kwok, S Lammel, D Lincoln, R Lipton, T Liu, C Madrid, K Maeshima, C Mantilla, D Mason, P McBride, P Merkel, S Mrenna, S Nahn, J Ngadiuba, D Noonan, V Papadimitriou, N Pastika, K Pedro, C Pena[85], F Ravera, A Reinsvold Hall[86], L Ristori, E Sexton-Kennedy, N Smith, A Soha, L Spiegel, S Stoynev, J Strait, L Taylor, S Tkaczyk, N V Tran, L Uplegger, E W Vaandering, I Zoi
Fermi National Accelerator Laboratory, Batavia, Illinois, United States of America

C Aruta, P Avery, D Bourilkov, L Cadamuro, P Chang, V Cherepanov, R D Field, E Koenig, M Kolosova, J Konigsberg, A Korytov, K H Lo, K Matchev, N Menendez, G Mitselmakher, K Mohrman, A Muthirakalayil Madhu, N Rawal, D Rosenzweig, S Rosenzweig, K Shi, J Wang
University of Florida, Gainesville, Florida, United States of America

T Adams, A Al Kadhim, A Askew, S Bower, R Habibullah, V Hagopian, R Hashmi, R.S Kim, S Kim, T Kolberg, G Martinez, H Prosper, P R Prova, M Wulansatiti, R Yohay, J Zhang
Florida State University, Tallahassee, Florida, United States of America

B Alsufyani, M M Baarmand, S Butalla, T Elkafrawy[20], M Hohlmann, R Kumar Verma, M Rahmani, E Yanes
Florida Institute of Technology, Melbourne, Florida, United States of America

M R Adams, A Baty, C Bennett, R Cavanaugh, R Escobar Franco, O Evdokimov, C E Gerber, D J Hofman, J h Lee, D S Lemos, A H Merrit, C Mills, S Nanda, G Oh, B Ozek, D Pilipovic, R Pradhan, T Roy, S Rudrabhatla, M B Tonjes, N Varelas, Z Ye, J Yoo
University of Illinois Chicago, Chicago, United States of America, Chicago, United States of America

M Alhusseini, D Blend, K Dilsiz[87], L Emediato, G Karaman, O K Köseyan, J -P Merlo, A Mestvirishvili[88], J Nachtman, O Neogi, H Ogul[89], Y Onel, A Penzo, C Snyder, E Tiras[90]
The University of Iowa, Iowa City, Iowa, United States of America

B Blumenfeld, L Corcodilos, J Davis, A V Gritsan, L Kang, S Kyriacou, P Maksimovic, M Roguljic, J Roskes, S Sekhar, M Swartz

Johns Hopkins University, Baltimore, Maryland, United States of America

A Abreu, L F Alcerro Alcerro, J Anguiano, P Baringer, A Bean, Z Flowers, D Grove, J King, G Krintiras, M Lazarovits, C Le Mahieu, C Lindsey, J Marquez, N Minafra, M Murray, M Nickel, M Pitt, S Popescu[91], C Rogan, C Royon, R Salvatico, S Sanders, C Smith, Q Wang, G Wilson
The University of Kansas, Lawrence, Kansas, United States of America

B Allmond, A Ivanov, K Kaadze, A Kalogeropoulos, D Kim, Y Maravin, K Nam, J Natoli, D Roy, G Sorrentino
Kansas State University, Manhattan, Kansas, United States of America

F Rebassoo, D Wright
Lawrence Livermore National Laboratory, Livermore, California, United States of America

A Baden, A Belloni, Y M Chen, S C Eno, N J Hadley, S Jabeen, R G Kellogg, T Koeth, Y Lai, S Lascio, A C Mignerey, S Nabili, C Palmer, C Papageorgakis, M M Paranjpe, L Wang
University of Maryland, College Park, Maryland, United States of America

J Bendavid, I A Cali, M D'Alfonso, J Eysermans, C Freer, G Gomez-Ceballos, M Goncharov, G Grosso, P Harris, D Hoang, D Kovalskyi, J Krupa, L Lavezzo, Y -J Lee, K Long, C Mironov, A Novak, C Paus, D Rankin, C Roland, G Roland, S Rothman, G S F Stephans, Z Wang, B Wyslouch, T J Yang
Massachusetts Institute of Technology, Cambridge, Massachusetts, United States of America

B Crossman, B M Joshi, C Kapsiak, M Krohn, D Mahon, J Mans, B Marzocchi, S Pandey, M Revering, R Rusack, R Saradhy, N Schroeder, N Strobbe, M A Wadud
University of Minnesota, Minneapolis, Minnesota, United States of America

L M Cremaldi
University of Mississippi, Oxford, Mississippi, United States of America

K Bloom, D R Claes, G Haza, J Hossain, C Joo, I Kravchenko, J E Siado, W Tabb, A Vagnerini, A Wightman, F Yan, D Yu
University of Nebraska-Lincoln, Lincoln, Nebraska, United States of America

H Bandyopadhyay, L Hay, I Iashvili, A Kharchilava, M Morris, D Nguyen, S Rappoccio, H Rejeb Sfar, A Williams
State University of New York at Buffalo, Buffalo, New York, United States of America

G Alverson, E Barberis, J Dervan, Y Haddad, Y Han, A Krishna, J Li, M Lu, G Madigan, R Mccarthy, D.M Morse, V Nguyen, T Orimoto, A Parker, L Skinnari, A Tishelman-Charny, B Wang, D Wood
Northeastern University, Boston, Massachusetts, United States of America

S Bhattacharya, J Bueghly, Z Chen, S Dittmer, K A Hahn, Y Liu, Y Miao, D G Monk, M H Schmitt, A Taliercio, M Velasco
Northwestern University, Evanston, Illinois, United States of America

G Agarwal, R Band, R Bucci, S Castells, A Das, R Goldouzian, M Hildreth, K W Ho, K Hurtado Anampa, T Ivanov, C Jessop, K Lannon, J Lawrence, N Loukas, L Lutton, J Mariano, N Marinelli, I Mcalister, T McCauley, C Mcgrady, C Moore, Y Musienko[16], H Nelson, M Osherson, A Piccinelli, R Ruchti, A Townsend, Y Wan, M Wayne, H Yockey, M Zarucki, L Zygala
University of Notre Dame, Notre Dame, Indiana, United States of America

A Basnet, B Bylsma, M Carrigan, L S Durkin, C Hill, M Joyce, M Nunez Ornelas, K Wei, B.L Winer, B R Yates
The Ohio State University, Columbus, Ohio, United States of America

F M Addesa, H Bouchamaoui, P Das, G Dezoort, P Elmer, A Frankenthal, B Greenberg, N Haubrich, G Kopp, S Kwan, D Lange, A Loeliger, D Marlow, I Ojalvo, J Olsen, A Shevelev, D Stickland, C Tully
Princeton University, Princeton, New Jersey, United States of America

S Malik
University of Puerto Rico, Mayaguez, Puerto Rico, United States of America

A S Bakshi, V E Barnes, S Chandra, R Chawla, S Das, A Gu, L Gutay, M Jones, A W Jung, D Kondratyev, A M Koshy, M Liu, G Negro, N Neumeister, G Paspalaki, S Piperov, V Scheurer, J F Schulte, M Stojanovic, J Thieman, A K Virdi, F Wang, W Xie
Purdue University, West Lafayette, Indiana, United States of America

J Dolen, N Parashar, A Pathak
Purdue University Northwest, Hammond, Indiana, United States of America

D Acosta, T Carnahan, K M Ecklund, P J Fernández Manteca, S Freed, P Gardner, F J M Geurts, W Li, O Miguel Colin, B P Padley, R Redjimi, J Rotter, E Yigitbasi, Y Zhang
Rice University, Houston, Texas, United States of America

A Bodek, P de Barbaro, R Demina, J L Dulemba, A Garcia-Bellido, O Hindrichs, A Khukhunaishvili, N Parmar, P Parygin[92], E Popova[92], R Taus
University of Rochester, Rochester, New York, United States of America

K Goulianos
The Rockefeller University, New York, New York, United States of America

B Chiarito, J P Chou, Y Gershtein, E Halkiadakis, M Heindl, D Jaroslawski, O Karacheban[30], I Laflotte, A Lath, R Montalvo, K Nash, H Routray, S Salur, S Schnetzer, S Somalwar, R Stone, S A Thayil, S Thomas, J Vora, H Wang
Rutgers, The State University of New Jersey, Piscataway, New Jersey, United States of America

H Acharya, D Ally, A G Delannoy, S Fiorendi, S Higginbotham, T Holmes, A R Kanuganti, N Karunarathna, L Lee, E Nibigira, S Spanier
University of Tennessee, Knoxville, Tennessee, United States of America

D Aebi, M Ahmad, O Bouhali[93], R Eusebi, J Gilmore, T Huang, T Kamon[94], H Kim, S Luo, R Mueller, D Overton, D Rathjens, A Safonov
Texas A&M University, College Station, Texas, United States of America

N Akchurin, J Damgov, V Hegde, A Hussain, Y Kazhykarim, K Lamichhane, S W Lee, A Mankel, T Peltola, I Volobouev, A Whitbeck
Texas Tech University, Lubbock, Texas, United States of America

E Appelt, Y Chen, S Greene, A Gurrola, W Johns, R Kunnawalkam Elayavalli, A Melo, F Romeo, P Sheldon, S Tuo, J Velkovska, J Viinikainen
Vanderbilt University, Nashville, Tennessee, United States of America

B Cardwell, B Cox, J Hakala, R Hirosky, A Ledovskoy, C Neu, C E Perez Lara
University of Virginia, Charlottesville, Virginia, United States of America

P E Karchin
Wayne State University, Detroit, Michigan, United States of America

A Aravind, S Banerjee, K Black, T Bose, S Dasu, I De Bruyn, P Everaerts, C Galloni, H He, M Herndon, A Herve, C K Koraka, A Lanaro, R Loveless, J Madhusudanan Sreekala, A Mallampalli, A Mohammadi, S Mondal, G Parida, L Pétré, D Pinna, A Savin, V Shang, V Sharma, W H Smith, D Teague, H.F Tsoi, W Vetens, A Warden
University of Wisconsin - Madison, Madison, Wisconsin, United States of America

S Afanasiev, V Andreev, Yu Andreev, T Aushev, M Azarkin, A Babaev, A Belyaev, V Blinov[95], E Boos, V Borshch, D Budkouski, V Bunichev, V Chekhovsky, R Chistov[95], M Danilov[95], A Dermenev, T Dimova[95], D Druzhkin[96], M Dubinin[85], L Dudko, A Ershov, G Gavrilov, V Gavrilov, S Gninenko, V Golovtcov, N Golubev, I Golutvin, I Gorbunov, A Gribushin, Y Ivanov, V Kachanov, V Karjavine, A Karneyeu, V Kim[95], M Kirakosyan, D Kirpichnikov, M Kirsanov, V Klyukhin, O Kodolova[97], V Korenkov, A Kozyrev[95], N Krasnikov, A Lanev, P Levchenko[98], N Lychkovskaya, V Makarenko, A Malakhov, V Matveev[95], V Murzin, A Nikitenko[99,97], S Obraztsov, V Oreshkin, V Palichik, V Perelygin, S Petrushanko, S Polikarpov[95], V Popov, O Radchenko[95], M Savina, V Savrin, V Shalaev, S Shmatov, S Shulha, Y Skovpen[95], S Slabospitskii, V Smirnov, A Snigirev, D Sosnov, V Sulimov, E Tcherniaev, A Terkulov, O Teryaev, I Tlisova, A Toropin, L Uvarov, A Uzunian, A Vorobyev†, N Voytishin, B S Yuldashev[100], A Zarubin, I Zhizhin, A Zhokin
Authors affiliated with an institute or an international laboratory covered by a cooperation agreement with CERN

† Deceased
[1]Also at Yerevan State University, Yerevan, Armenia
[2]Also at TU Wien, Vienna, Austria
[3]Also at Institute of Basic and Applied Sciences, Faculty of Engineering, Arab Academy for Science, Technology and Maritime Transport, Alexandria, Egypt
[4]Also at Ghent University, Ghent, Belgium
[5]Also at Universidade Estadual de Campinas, Campinas, Brazil
[6]Also at Federal University of Rio Grande do Sul, Porto Alegre, Brazil
[7]Also at UFMS, Nova Andradina, Brazil
[8]Also at Nanjing Normal University, Nanjing, People's Republic of China
[9]Now at The University of Iowa, Iowa City, Iowa, United States of America

[10]Also at University of Chinese Academy of Sciences, Beijing, People's Republic of China
[11]Also at People's Republic of China Center of Advanced Science and Technology, Beijing, People's Republic of China
[12]Also at University of Chinese Academy of Sciences, Beijing, People's Republic of China
[13]Also at People's Republic of China Spallation Neutron Source, Guangdong, People's Republic of China
[14]Now at Henan Normal University, Xinxiang, People's Republic of China
[15]Also at Université Libre de Bruxelles, Bruxelles, Belgium
[16]Also at an institute or an international laboratory covered by a cooperation agreement with CERN
[17]Also at Helwan University, Cairo, Egypt
[18]Now at Zewail City of Science and Technology, Zewail, Egypt
[19]Also at British University in Egypt, Cairo, Egypt
[20]Now at Ain Shams University, Cairo, Egypt
[21]Also at Purdue University, West Lafayette, Indiana, United States of America
[22]Also at Université de Haute Alsace, Mulhouse, France
[23]Also at Department of Physics, Tsinghua University, Beijing, People's Republic of China
[24]Also at The University of the State of Amazonas, Manaus, Brazil
[25]Also at Erzincan Binali Yildirim University, Erzincan, Turkey
[26]Also at University of Hamburg, Hamburg, Germany
[27]Also at RWTH Aachen University, III. Physikalisches Institut A, Aachen, Germany
[28]Also at Isfahan University of Technology, Isfahan, Iran
[29]Also at Bergische University Wuppertal (BUW), Wuppertal, Germany
[30]Also at Brandenburg University of Technology, Cottbus, Germany
[31]Also at Forschungszentrum Jülich, Juelich, Germany
[32]Also at CERN, European Organization for Nuclear Research, Geneva, Switzerland
[33]Also at Institute of Physics, University of Debrecen, Debrecen, Hungary
[34]Also at Institute of Nuclear Research ATOMKI, Debrecen, Hungary
[35]Now at Universitatea Babes-Bolyai - Facultatea de Fizica, Cluj-Napoca, Romania
[36]Also at Physics Department, Faculty of Science, Assiut University, Assiut, Egypt
[37]Also at HUN-REN Wigner Research Centre for Physics, Budapest, Hungary
[38]Also at Punjab Agricultural University, Ludhiana, India
[39]Also at University of Visva-Bharati, Santiniketan, India
[40]Also at Indian Institute of Science (IISc), Bangalore, India
[41]Also at Birla Institute of Technology, Mesra, Mesra, India
[42]Also at IIT Bhubaneswar, Bhubaneswar, India
[43]Also at Institute of Physics, Bhubaneswar, India
[44]Also at University of Hyderabad, Hyderabad, India
[45]Also at Deutsches Elektronen-Synchrotron, Hamburg, Germany
[46]Also at Department of Physics, Isfahan University of Technology, Isfahan, Iran
[47]Also at Sharif University of Technology, Tehran, Iran
[48]Also at Department of Physics, University of Science and Technology of Mazandaran, Behshahr, Iran
[49]Also at Italian National Agency for New Technologies, Energy and Sustainable Economic Development, Bologna, Italy
[50]Also at Centro Siciliano di Fisica Nucleare e di Struttura Della Materia, Catania, Italy
[51]Also at Università degli Studi Guglielmo Marconi, Roma, Italy
[52]Also at Scuola Superiore Meridionale, Università di Napoli 'Federico II', Napoli, Italy
[53]Also at Fermi National Accelerator Laboratory, Batavia, Illinois, United States of America
[54]Also at Consiglio Nazionale delle Ricerche - Istituto Officina dei Materiali, Perugia, Italy
[55]Also at Riga Technical University, Riga, Latvia
[56]Also at Department of Applied Physics, Faculty of Science and Technology, Universiti Kebangsaan Malaysia, Bangi, Malaysia
[57]Also at Consejo Nacional de Ciencia y Tecnología, Mexico City, Mexico
[58]Also at Trincomalee Campus, Eastern University, Sri Lanka, Nilaveli, Sri Lanka
[59]Also at Saegis Campus, Nugegoda, Sri Lanka
[60]Also at National and Kapodistrian University of Athens, Athens, Greece
[61]Also at Ecole Polytechnique Fédérale LaUnited States of Americanne, LaUnited States of Americanne, Switzerland
[62]Also at Universität Zürich, Zurich, Switzerland
[63]Also at Stefan Meyer Institute for Subatomic Physics, Vienna, Austria
[64]Also at Laboratoire d'Annecy-le-Vieux de Physique des Particules, IN2P3-CNRS, Annecy-le-Vieux, France
[65]Also at Near East University, Research Center of Experimental Health Science, Mersin, Turkey
[66]Also at Konya Technical University, Konya, Turkey
[67]Also at Izmir Bakircay University, Izmir, Turkey
[68]Also at Adiyaman University, Adiyaman, Turkey
[69]Also at Bozok Universitetesi Rektörlügü, Yozgat, Turkey
[70]Also at Marmara University, Istanbul, Turkey
[71]Also at Milli Savunma University, Istanbul, Turkey
[72]Also at Kafkas University, Kars, Turkey
[73]Now at stanbul Okan University, Istanbul, Turkey
[74]Also at Hacettepe University, Ankara, Turkey
[75]Also at Istanbul University - Cerrahpasa, Faculty of Engineering, Istanbul, Turkey
[76]Also at Yildiz Technical University, Istanbul, Turkey
[77]Also at Vrije Universiteit Brussel, Brussel, Belgium
[78]Also at School of Physics and Astronomy, University of Southampton, Southampton, United Kingdom
[79]Also at University of Bristol, Bristol, United Kingdom
[80]Also at IPPP Durham University, Durham, United Kingdom
[81]Also at Monash University, Faculty of Science, Clayton, Australia

[82]Also at Università di Torino, Torino, Italy
[83]Also at Bethel University, St. Paul, Minnesota, United States of America
[84]Also at Karamanoğlu Mehmetbey University, Karaman, Turkey
[85]Also at California Institute of Technology, Pasadena, California, United States of America
[86]Also at United States Naval Academy, Annapolis, Maryland, United States of America
[87]Also at Bingol University, Bingol, Turkey
[88]Also at Georgian Technical University, Tbilisi, Georgia
[89]Also at Sinop University, Sinop, Turkey
[90]Also at Erciyes University, Kayseri, Turkey
[91]Also at Horia Hulubei National Institute of Physics and Nuclear Engineering (IFIN-HH), Bucharest, Romania
[92]Now at an institute or an international laboratory covered by a cooperation agreement with CERN
[93]Also at Texas A&M University at Qatar, Doha, Qatar
[94]Also at Kyungpook National University, Daegu, Republic of Korea
[95]Also at another institute or international laboratory covered by a cooperation agreement with CERN
[96]Also at Universiteit Antwerpen, Antwerpen, Belgium
[97]Also at Yerevan Physics Institute, Yerevan, Armenia
[98]Also at Northeastern University, Boston, Massachusetts, United States of America
[99]Also at Imperial College, London, United Kingdom
[100]Also at Institute of Nuclear Physics of the Uzbekistan Academy of Sciences, Tashkent, Uzbekistan

References

[1] Glashow S L 1961 Partial symmetries of weak interactions *Nucl. Phys.* **22** 579
[2] Weinberg S 1967 A model of leptons *Phys. Rev. Lett.* **19** 1264
[3] Salam A 1968 Weak and electromagnetic interactions *Proc. 8th Nobel Symp. N* Svartholm (Almqvist and Wiksell) p 367
[4] Particle Data Group 2022 Review of particle physics *Prog. Theor. Exp. Phys.* **2022** 083C01
[5] ALEPH, DELPHI, L3, OPAL, LEP Electroweak Collaboration 2013 Electroweak measurements in electron-positron collisions at W-boson-pair energies at LEP *Phys. Rep.* **532** 119
[6] ATLAS Collaboration 2021 Test of the universality of τ and μ lepton couplings in W-boson decays with the ATLAS detector *Nat. Phys.* **17** 813
[7] CMS Collaboration 2022 Precision measurement of the W boson decay branching fractions in proton-proton collisions at $\sqrt{s} = 13$ TeV *Phys. Rev.* D **105** 072008
[8] London D and Matias J 2022 *B* flavour anomalies: 2021 theoretical status report *Annu. Rev. Nucl. Part. Sci.* **72** 37
[9] LHCb Collaboration 2022 Test of lepton universality in beauty-quark decays *Nat. Phys.* **18** 277
[10] CLEO Collaboration 2007 First observation of $\Upsilon(3S) \to \tau^+\tau^-$ and tests of lepton universality in Υ decays *Phys. Rev. Lett.* **98** 052002
[11] BaBar Collaboration 2010 Test of lepton universality in $\Upsilon(1S)$ decays at BaBar *Phys. Rev. Lett.* **104** 191801
[12] BaBar Collaboration 2012 Measurement of branching fractions and rate asymmetries in the rare decays $B \to K^{(*)}\ell^+\ell^-$ *Phys. Rev.* D **86** 032012
[13] BESIII Collaboration 2019 Study of the $D^0 \to K^-\mu^+\nu_\mu$ dynamics and test of lepton flavor universality with $K^-\ell^+\nu_\ell$ decays *Phys. Rev. Lett.* **122** 011804
[14] Belle Collaboration 2021 Test of lepton-flavor universality in $B \to K^*\ell^+\ell^-$ decays at Belle *Phys. Rev. Lett.* **126** 161801
[15] Belle Collaboration 2021 Test of lepton flavor universality and search for lepton flavor violation in $B \to K\ell\ell$ decays *J. High Energy Phys.* JHEP03(2021)105
[16] Belle Collaboration 2022 First test of lepton flavor universality in the charmed baryon decays $\Omega_c^0 \to \Omega^-\ell^+\nu_\ell$ using data of the Belle experiment *Phys. Rev.* D **105** L091101
[17] BESIII Collaboration 2023 Study of $\Lambda_c^+ \to \Lambda\mu^+\nu_\mu$ and test of lepton flavor universality with $\Lambda_c^+ \to \Lambda\ell^+\nu_\ell$ decays (arXiv:2306.02624)
[18] BESIII Collaboration 2024 Test of lepton universality and measurement of the form factors of $D^0 \to K^*(892)^-\mu^+\nu_\mu$ (arXiv:2403.10877)
[19] LHCb Collaboration 2014 Test of lepton universality using $B^+ \to K^+\ell^+\ell^-$ decays *Phys. Rev. Lett.* **113** 151601
[20] LHCb Collaboration 2019 Search for lepton-universality violation in $B^+ \to K^+\ell^+\ell^-$ decays *Phys. Rev. Lett.* **122** 191801
[21] LHCb Collaboration 2017 Test of lepton universality with $B^0 \to K^{*0}\ell^+\ell^-$ decays *J. High Energy Phys.* JHEP08(2017)055
[22] LHCb Collaboration 2022 Tests of lepton universality using $B^0 \to K_S^0\ell^+\ell^-$ and $B^+ \to K^{*+}\ell^+\ell^-$ decays *Phys. Rev. Lett.* **128** 191802
[23] LHCb Collaboration 2012 Measurement of the isospin asymmetry in $B \to K^{(*)}\mu^+\mu^-$ decays *J. High Energy Phys.* JHEP07(2012)133
[24] LHCb Collaboration 2014 Differential branching fractions and isospin asymmetries of $B \to K^{(*)}\mu^+\mu^-$ decays *J. High Energy Phys.* JHEP06(2014)133
[25] LHCb Collaboration 2016 Measurements of the S-wave fraction in $B^0 \to K^+\pi^-\mu^+\mu^-$ decays and the $B^0 \to K^*(892)^0\mu^+\mu^-$ differential branching fraction *J. High Energy Phys.* JHEP11(2016)047
[26] LHCb Collaboration 2021 Branching fraction measurements of the rare $B_s^0 \to \phi\mu^+\mu^-$ and $B_s^0 \to f_2'(1525)\mu^+\mu^-$ decays *Phys. Rev. Lett.* **127** 151801
[27] Ciuchini M, Fedele M, Franco E, Paul A, Silvestrini L and Valli M 2023 Charming penguins and lepton universality violation in $b \to s\ell^+\ell^-$ decays *Eur. Phys. J.* C **83** 64
[28] Gubernari N, Reboud M, van Dyk D and Virto J 2023 Dispersive analysis of $B \to K^{(*)}$ and $B_s \to \phi$ form factors (arXiv:2305.06301)
[29] Gubernari N 2024 Theoretical predictions for $b \to s\mu^+\mu^-$ decays *58th Rencontres de Moriond on Cosmology* (arXiv:2404.10043)
[30] LHCb Collaboration 2023 Test of lepton universality in $b \to s\ell^+\ell^-$ decays *Phys. Rev. Lett.* **131** 051803
[31] LHCb Collaboration 2023 Measurement of lepton universality parameters in $B^+ \to K^+\ell^+\ell^-$ and $B^0 \to K^{*0}\ell^+\ell^-$ decays *Phys. Rev.* D **108** 032002
[32] Patnaik S, Nayak L and Singh R 2023 Assessing lepton flavor universality violations in semileptonic decays (arXiv:2308.05677)
[33] 2024 HEPDATA record for this analysis (http://dx.doi.org/10.17182/hepdata.146018)
[34] Hiller G and Kruger F 2004 More model-independent analysis of $b \to s$ processes *Phys. Rev.* D **69** 074020

[35] Bordone M, Isidori G and Pattori A 2016 On the standard model predictions for R_K and R_{K^*} *Eur. Phys. J.* C **76** 440

[36] Isidori G, Nabeebaccus S and Zwicky R 2020 QED corrections in $\overline{B} \to \overline{K}\ell^+\ell^-$ at the double-differential level *J. High Energy Phys.* JHEP12(2020)104

[37] Isidori G, Lancierini D, Nabeebaccus S and Zwicky R 2022 QED in $\overline{B} \to \overline{K}\ell^+\ell^-$ LFU ratios: theory versus experiment, a Monte Carlo study *J. High Energy Phys.* JHEP10(2022)146

[38] Roodman A 2003 Blind analysis in particle physics (arXiv:physics/0312102)

[39] CMS Collaboration 2022 Strategies and performance of the CMS silicon tracker alignment during LHC Run 2 *Nucl. Instrum. Methods Phys. Res.* A **1037** 166795

[40] CMS Tracker Group Collaboration 2021 The CMS Phase-1 pixel detector upgrade *J. Instrum.* **16** P02027

[41] CMS Collaboration 2020 Track impact parameter resolution for the full pseudo rapidity coverage in the 2017 dataset with the CMS Phase-1 pixel detector *CMS Detector Performance Summary* CMS-DP-2020-049 (available at: https://cds.cern.ch/record/2743740)

[42] CMS Collaboration 2018 Performance of the CMS muon detector and muon reconstruction with proton-proton collisions at $\sqrt{s} = 13$ TeV *J. Instrum.* **13** P06015

[43] CMS Collaboration 2021 Electron and photon reconstruction and identification with the CMS experiment at the CERN LHC *J. Instrum.* **16** P05014

[44] CMS Collaboration 2019 Recording and reconstructing 10 billion unbiased B hadron decays in CMS *CMS Detector Performance Summary* CMS-DP-2019-043 (available at: https://cds.cern.ch/record/2704495)

[45] CMS Collaboration 2024 Enriching the physics program of the CMS experiment via data scouting and data parking (arXiv:2403.16134 [hep-ex])

[46] CMS Collaboration 2020 ECAL 2016 refined calibration and Run 2 summary plots *CMS Detector Performance Summary* CMS-DP-2020-021 (available at: https://cds.cern.ch/record/2717925)

[47] CMS Collaboration 2020 Performance of the CMS Level-1 trigger in proton-proton collisions at $\sqrt{s} = 13$ TeV *J. Instrum.* **15** P10017

[48] CMS Collaboration 2017 The CMS trigger system *J. Instrum.* **12** P01020

[49] CMS Collaboration 2008 The CMS experiment at the CERN LHC *J. Instrum.* **3** S08004

[50] CMS Collaboration 2014 Description and performance of track and primary-vertex reconstruction with the CMS tracker *J. Instrum.* **9** P10009

[51] CMS Collaboration 2018 CMS luminosity measurements for the 2018 data-taking period at $\sqrt{s} = 13$ TeV *CMS Physics Analysis Summary* CMS-PAS-LUM-18-001 (available at: https://cds.cern.ch/record/2676164)

[52] Sjöstrand T , Ask S, Christiansen J R, Corke R, Desai N, Ilten P, Mrenna S, Prestel S, Rasmussen C O and Skands P Z 2015 An introduction to PYTHIA 8.2 *Comput. Phys. Commun.* **191** 159

[53] Lange D J 2001 The EvtGen particle decay simulation package *Nucl. Instrum. Methods Phys. Res.* A **462** 152

[54] CMS Collaboration 2020 Extraction and validation of a new set of CMS PYTHIA8 tunes from underlying-event measurements *Eur. Phys. J.* C **80** 4

[55] NNPDF Collaboration 2017 Parton distributions from high-precision collider data *Eur. Phys. J.* C **77** 663

[56] Barberio E and Waş Z 1994 PHOTOS: a universal Monte Carlo for QED radiative corrections. Version 2.0 *Comput. Phys. Commun.* **79** 291

[57] Ball P and Zwicky R 2005 $B_{d,s} \to \rho, \omega, K^*, \phi$ decay form-factors from light-cone sum rules revisited *Phys. Rev.* D **71** 014029

[58] Bharucha A, Straub D M and Zwicky R 2016 $B \to V\ell^+\ell^-$ in the standard model from light-cone sum rules *J. High Energy Phys.* JHEP08(2016)098

[59] Gubernari N, Kokulu A and van Dyk D 2019 $B \to P$ and $B \to V$ form factors from B-meson light-cone sum rules beyond leading twist *J. High Energy Phys.* JHEP01(2019)150

[60] HPQCD Collaboration 2023 $B \to K$ and $D \to K$ form factors from fully relativistic lattice QCD *Phys. Rev.* D **107** 014510

[61] GEANT4 Collaboration 2003 GEANT4—a simulation toolkit *Nucl. Instrum. Methods Phys. Res.* A **506** 250

[62] CMS Collaboration 2017 Particle-flow reconstruction and global event description with the CMS detector *J. Instrum.* **12** P10003

[63] Chen T and Guestrin C 2016 XGBoost: a scalable tree boosting system (arXiv:1603.02754)

[64] CMS Collaboration 2011 Measurements of inclusive W and Z cross sections in pp collisions at $\sqrt{s} = 7$ TeV *J. High Energy Phys.* JHEP01(2011)080

[65] CMS Collaboration 2010 CMS tracking performance results from early LHC operation *Eur. Phys. J.* C **70** 1165

[66] Prokofiev K and Speer T 2005 A kinematic fit and a decay chain reconstruction library *Proc. Computing in High Energy and Nuclear Physics 2004* vol 1 p CERN-2005-002 (http://dx.doi.org/10.5170/CERN-2005-002.411)

[67] Pivk M and Le Diberder F R 2005 ${}_s\mathcal{P}$lot: a statistical tool to unfold data distributions *Nucl. Instrum. Methods Phys. Res.* A **555** 356

[68] Cacciari M, Greco M and Nason P 1998 The p_T spectrum in heavy-flavour hadroproduction *J. High Energy Phys.* JHEP05(1998)007

[69] Cacciari M, Frixione S and Nason P 2001 The p_T spectrum in heavy-flavour photoproduction *J. High Energy Phys.* JHEP03(2001)006

[70] Cacciari M , Frixione S, Houdeau N, Mangano M L, Nason P and Ridolfi G 2012 Theoretical predictions for charm and bottom production at the LHC *J. High Energy Phys.* JHEP10(2012)137

[71] Cacciari M, Mangano M L and Nason P 2015 Gluon PDF constraints from the ratio of forward heavy-quark production at the LHC at $\sqrt{s} = 7$ and 13 TeV *Eur. Phys. J.* C **75** 610

[72] Oreglia M J 1980 A study of the reactions $\psi' \to \gamma\gamma\psi$ *PhD Thesis* Stanford University (available at: www.slac.stanford.edu/pubs/cgi-wrap/getdoc/slac-r-236.pdf)

[73] Gaiser J E 1982 Charmonium spectroscopy from radiative decays of J/ψ and ψ' *PhD Thesis* Stanford University (available at: www.slac.stanford.edu/cgi-bin/getdoc/slac-r-255.pdf)

[74] Cranmer K S 2001 Kernel estimation in high-energy physics *Comput. Phys. Commun.* **136** 198

[75] CMS Collaboration 2018 Measurement of the inelastic proton-proton cross section at $\sqrt{s} = 13$ TeV *J. High Energy Phys.* JHEP07(2018)161

[76] de Blas J *et al* 2020 `HEPfit`: a code for the combination of indirect and direct constraints on high energy physics models *Eur. Phys. J.* C **80** 456

[77] Alasfar L *et al* 2020 *B* anomalies under the lens of electroweak precision *J. High Energy Phys.* JHEP12(2020)016

[78] Ciuchini M , Fedele M, Franco E, Paul A, Silvestrini L and Valli M 2023 Constraints on lepton universality violation from rare B decays *Phys. Rev.* D **107** 055036

[79] Mahmoudi F 2008 SuperIso: a program for calculating the isospin asymmetry of $B \to K^* \gamma$ in the MSSM *Comput. Phys. Commun.* **178** 745
[80] Mahmoudi F 2009 SuperIso v2.3: a program for calculating flavor physics observables in supersymmetry *Comput. Phys. Commun.* **180** 1579
[81] Straub D M 2018 flavio: a Python package for flavour and precision phenomenology in the standard model and beyond (arXiv:1810.08132)
[82] EOS Collaboration 2022 EOS: a software for flavor physics phenomenology *Eur. Phys. J.* C **82** 569
[83] Gubernari N, Reboud M, van Dyk D and Virto J 2022 Improved theory predictions and global analysis of exclusive $b \to s\mu^+\mu^-$ processes *J. High Energy Phys.* JHEP09(2022)133
[84] LHCb Collaboration 2017 Measurement of the phase difference between short- and long-distance amplitudes in the $B^+ \to K^+\mu^+\mu^-$ decay *Eur. Phys. J.* C **77** 161